From THE DEPARTMENT OF CLINICAL NEUROSCIENCE
Karolinska Institutet, Stockholm, Sweden

CEREBRAL BLOOD FLOW AND GLUCOSE METABOLISM IN ISCHEMIC STROKE

MULTIMODAL IMAGING INVESTIGATIONS IN A CLINICALLY RELEVANT RAT MODEL

Fabian Arnberg

Stockholm 2015

Published by Karolinska Institutet.
Printed by E-print AB 2015
Cover art: Collaged images from experiments performed during the thesis work.

ISBN 978-91 -7676-116-8

CEREBRAL BLOOD FLOW AND GLUCOSE METABOLISM IN ISCHEMIC STROKE

Multimodal Imaging Investigations in a Clinically Relevant Rat Model

THESIS FOR DOCTORAL DEGREE (Ph.D.)

By

Fabian Arnberg

Principal Supervisor:
Prof. Staffan Holmin
Karolinska Institutet
Department of Clinical Neuroscience

Co-supervisor:
Associate Prof. Michael Söderman
Karolinska Institutet
Department of Clinical Neuroscience

Opponent:
Prof. Andreas Meisel
Charité Universitätsmedizin, Berlin, Germany
Department of Neurology
Division of Experimental Neurology

Examination Board:
Associate Prof. Fredrik Lennmyr
Uppsala University
Department of Surgical Sciences
Section of Anaesthiology and Critical Care

Prof. Pia Sundgren
Lund University
Department of Medicine
Department of Diagnostic Radiology

Prof. Lars Olson
Karolinska Institutet
Department of Neuroscience

To Jessika, Elmer, Tyra and Hedvig

ABSTRACT

Ischemic stroke is one of the leading causes of death worldwide. Ischemic stroke is also a major cause of long-term disability with vast socioeconomic results for patients, their relatives and health services. Over the last decades, experimental research has resulted in significant progress of our understanding of mechanisms leading to brain injury after ischemic stroke. However, so far, translational research targeting these mechanisms has failed. This failure has resulted in a general consensus that a more integrative approach is needed to account for not only neurobiology under ischemia, but also the ischemic impact on the neurovascular interface. Accordingly, new tools for simultaneously imaging and perturbing this interface needs to be established. The aims of the present work were firstly to develop an ischemic stroke model in rats that more closely mimics human stroke. Secondly, our goal was to incorporate the model with perfusion- and metabolic imaging using high-field magnetic resonance imaging (HF-MRI) and positron emission tomography (PET). Finally we wanted to apply the model in a treatment study targeting the neurovascular interface, and use HF-MRI and PET to assess treatment outcome.

We translated endovascular techniques from bedside to bench in the interest of realizing a new rat model for focal cerebral ischemia, in which a microwire is navigated under X-ray fluoroscopy to an occluding position in the middle cerebral artery (MCA). Furthermore, we were able to use the endovascular technique to facilitate intra-arterial microcatheter access to the cerebrovascular system in the rat accommodating injections with varying degree of selectivity. Next, we established protocols for HF-MRI and PET to obtain imaging of pathophysiological events following acute and subacute ischemic stroke. Finally we applied the aforementioned techniques in a treatment study targeting vascular endothelial growth factor B (VEGF-B) in ischemic stroke.

We found that the translation of clinical endovascular techniques to the experimental setting opened up several possibilities to access and perturb the neurovascular interface. In comparison with earlier models for focal stroke in the rat, the model for ischemic stroke presented in Paper I produces an injury and pathophysiology more resembling human stroke. Furthermore, the model showed to be highly compatible with small animal imaging systems with the possibility to occlude the MCA and to inject substances directly to the cerebrovascular supply before, during and after imaging (Paper II). The model also makes it possible to control blood flow during scanning with various modalities. HF-MRI and [2-^{18}F]-2-Fluoro-2-deoxy-D-glucose PET investigations of acute ischemia in Paper III provided evidence for hypermetabolism of glucose occurring in parallel with diffusion restriction of brain water, suggesting an extension of the current paradigm of the mechanisms behind infarct-related diffusion restriction of water. In Paper IV, we found that VEGF-B antagonism result in a reduction of stroke volume, indicating a mechanism of action of VEGF-B in ischemic stroke warranting further treatment studies targeting VEGF-B in ischemic stroke.

LIST OF SCIENTIFIC PAPERS

This thesis is based on the following papers:

I. **Arnberg F**, Lundberg J, Söderman M, Damberg P and Holmin S. Image-guided method in the rat for inducing cortical or striatal infarction and for controlling cerebral blood flow under MRI.
Stroke (2012).

II. **Arnberg F**, Samén E, Lundberg J, Lu L, Grafström J, Söderman M, Stone-Elander S and Holmin S. Selective intra-arterial administration of 18F-FDG to the rat brain - effects on hemispheric uptake.
Neuroradiology (2014)

III. **Arnberg F**, Grafström J, Lundberg J, Nikkhou-Aski S, Little P, Damberg P, Mitsios N, Mulder J, Lu L, Söderman M, Stone-Elander S and Holmin S. Imaging of a clinically relevant stroke model: glucose hypermetabolism revisited.
Stroke (2015)

IV. **Arnberg F**, Little P, Fredriksson L, Damberg P, Lu L, Nikkhou-Aski S, Söderman M, Stone-Elander S, Nilsson I, Eriksson U, and Holmin S. VEGF-B antagonism reduces infarct size in a rat model of stroke.
Manuscript.

Scientific papers by this author that are not part of this thesis:

I. Lindh C, Wennersten A, **Arnberg F**, Holmin S, Mathiesen T. Differences in cell death between high and low energy brain injury in adult rats. *Acta Neurochirurgica* (2008).

II. Zu S, Winberg J, **Arnberg F**, Palmer G, Svensson P-J, Wester T and Agneta Nordenskjöld. Mutation analysis of the motor neuron and pancreas homeobox 1 (MNX1, former HLXB9) gene in Swedish patients with Currarino syndrome. *Journal of Pediatric Surgery* (2011).

III. Nilsson I-L, **Arnberg F**, Zedenius J and Sundin A. Thyroid incidentaloma detected by fluorodeoxyglucose positron emission tomography/computed tomography: practical management algorithm. *World Journal of Surgery* (2011).

IV. **Arnberg F**, Gahm C, Mathiesen T. L-N-iminoethyl-lysine after experimental brain trauma attenuates cellular proliferation and astrocyte differentiation. *Acta Neurochirurgica* (2012).

V. Samen E, **Arnberg F**, Lu L, Olofsson MH, Tegnebratt T, Thorell JO, Holmin S and Stone-Elander S. Metabolism of epidermal growth factor receptor targeting probe [11C]PD153035: impact on biodistribution and tumor uptake in rats. *Journal of Nuclear Medicine* (2013).

VI. Majeed A, Meijer K, Larrazabal R, **Arnberg F**, Luijckx GJ, Roberts RS and Schulman S. Mortality in vitamin K antagonist-related intracerebral bleeding treated with plasma or 4-factor prothrombin complex concentrate. *Journal of Thrombosis and Haemostasis* (2014).

VII. **Arnberg F**, Lundberg J, Kenne E, Jaff N, Müller P, Nava S, Kaipe H, Ringdén, O and Holmin S. Superselective intra-arterial umbilical cord blood administration to BM in experimental animals. *Bone Marrow Transplantation* (2014).

VIII. Tóth M, Little P, **Arnberg F**, Häggkvist J, Mulder J, Halldin C, Gulyás B and Holmin S. Acute neuroinflammation in a clinically relevant focal cortical ischemic stroke model in rat: longitudinal positron emission tomography and immunofluorescent tracking. *Brain Structure and Function* (2015).

IX. **Arnberg F**, Lundberg J, Olsson A, Samén E, Jaff N, Jussing E, Dahlén U, Nava S, Axelsson R, Ringdén O, Kaipe H and Holmin S. Intra-arterial administration of placenta-derived decidual stromal cells to the superior mesenteric artery in the rabbit: distribution of cells, feasibility and safety *Cell Transplantation* (2015).

CONTENTS

LIST OF ABBREVIATIONS

[^{18}F]FDG	[2-^{18}F]-2-fluoro-2-deoxy-D-glucose
ACA	anterior cerebral artery
ADC	apparent diffusion coefficient
ASL	arterial spin labeling
CCA	common carotid artery
cICA	cervical segment of the internal carotid artery
DSA	digital subtraction angiography
DWI	diffusion-weighted imaging
EC	extracellular compartment
HF-MRI	high-field magnetic resonance imaging
IC	intracellular compartment
ICA	internal carotid artery
IHC	immunohistochemistry
iICA	intracranial internal carotid artery
ISO	isoflurane
IR	interventional radiology
MCA	middle cerebral artery
MCAO	middle cerebral artery occlusion
M2CAO	occlusion of segment 2 of the middle cerebral artery
MRI	magnetic resonance imaging
MRS	magnetic resonance spectroscopy
PComA	posterior communicating artery
PET	positron emission tomography
PPA	pterygopalatine artery
T1WI	T1-weighted imaging
T2WI	T2-weighted imaging
TE	echo time
TR	repetition time
VEGF-B	vascular endothelial growth factor b

1 INTRODUCTION

Although rates of stroke mortality have decreased worldwide in the past two decades, the number of people affected every year, related deaths and the overall burden of stroke is great and increasing (Feigin et al. 2014). If these trends continue, by 2030 there will globally be 12 million deaths caused by stroke, 70 million people surviving stroke and 200 million disability adjusted life years lost (Feigin et al. 2014). Among all factors contributing to stroke epidemiology, two important agents have come into play in developed countries. Firstly, reduction of stroke mortality and more favourable outcomes have been achieved by the organization of acute stroke care focusing on timely recanalization therapy by intravenous thrombolysis. Recently, even more favourable outcomes have been achieved by adding endovascular treatment to recanalization therapy (Berkhemer et al. 2015; Goyal et al. 2015; Saver et al. 2015; Campbell et al. 2013; Molina et al. 2013). The development of modern stroke management has relied heavily on the progress of neuroimaging, with a number of imaging protocols emerging during the last decades, notably computed tomography (CT) and magnetic resonance imaging (MRI). Today, there is a demand to further develop neuroimaging in order to more appropriately triage patients to tailored treatment protocols. The second agent impacting heavily on stroke epidemiology is the rapidly increasing prevalence of type 2 diabetes, one of the most important risk factors for ischemic stroke (Chen et al. 2012; Kissela et al. 2005). This thesis discusses how features of endovascular techniques, imaging and emerging treatments of type-2 diabetes can be incorporated into the experimental backbone of ischemic stroke research.

1.1 EXPERIMENTAL ISCHEMIC STROKE

1.1.1 Lost in translation

Animal models of ischemic stroke have played an important role in the discovery of pathophysiological concepts that have been proven clinically relevant. One salient example is how experimental studies established the concept of the ischemic penumbra, i.e. brain tissue with perfusion values between the flow threshold for reversible functional failure and the flow threshold for irreversible membrane failure (Astrup et al. 1977). However, despite the significant progress in understanding the pathophysiology of ischemic brain tissue injury and a large number of experimentally successful treatment studies, clinical translation into effective therapeutic measures has ultimately run into a "translational roadblock" (Endres et al. 2008; Dirnagl & Fisher 2012). Given the historical inability to successfully translate results from current experimental stroke models, it has been necessary to go back to the experimental drawing board.

1.1.2 Do we really need another mousetrap?

The rat is the most employed animal in experimental ischemic stroke studies due to low cost and because of a substantial cerebrovascular resemblance to humans (Macrae 1992). Among a wide array of rat models, the intraluminal suture model developed in the 1980's (Longa et

al. 1989; Koizumi et al. 1986) is, even today, the most frequently used (Durukan & Tatlisumak 2007). In this model, a monofilament is inserted into the internal carotid artery (ICA) and advanced until reaching the origin of the anterior cerebral artery (ACA), thereby blocking blood flow to the middle cerebral artery (MCA). Although this model has several advantages such as reproducibility, reliability and the option to perform permanent or transient occlusion, there are also several limitations to this procedure that hinder accurate modeling of treatable human stroke. The suture model causes large infarcts and has a high risk of hemorrhage (Carmichael 2006).

Since the initial presentation of the suture model by Koizumi in 1986 (Koizumi et al. 1986), several modifications have been performed with the aim of decreasing the risk of hemorrhage and to limit the size of infarcts. These modifications have largely aimed at improving the filament design, in order to limit the occlusion of arteries adjacent to the MCA (Longa et al. 1989; Belayev et al. 1996; Shimamura et al. 2006). There are important differences between humans and rats regarding the arterial supply of posterior- and subcortical brain regions (the posterior circulation). In rats, the main contributor to the posterior cerebral artery (PCA) is the posterior communicating artery (PComA), branching from the top of the ICA (Feigin et al. 2014; Brown 1966), whereas in humans the posterior circulation is most commonly supplied by the basilar artery. The intraluminal suture model causes occlusion of the PComA and the ACA, resulting in variable and widespread subcortical injury with delayed stroke progression more comparable to a terminal ICA occlusion (carotid T-occlusion) than middle cerebral artery occlusion (MCAO) (Kanemitsu et al. 2002). As ischemic brain injury has proven to be heterogenous in nature, there is an obvious problem if applying a model with the characteristics of a terminal ICA occlusion, when performing treatment studies aimed at ameliorating the most common macrovascular ischemic event in the human brain - MCAO.

1.2 EXPERIMENTAL ENDOVASCULAR METHODS

1.2.1 Navigating to the rat MCA under fluoroscopy

In the 1960's, interventional radiology (IR) was developed from diagnostic angiography. Today, IR has become a widely used therapeutic instrument for a number of diseases in many different fields of medicine. The technique allows X-Ray fluoroscopy guided catheter navigation to almost all parts of the vascular system in humans. Recently, IR has been explored as a tool to facilitate experimental stroke research (Divani et al. 2015; Shimamura et al. 2009; F. Sun et al. 2005). Fluoroscopic control has been reported to be useful in experimental stroke models, as the occluding filament can be positioned more accurately. Furthermore, fluoroscopic guidance allows insertion of the occluding filament in peripheral arteries with subsequent navigation to the circle of Willis. In the rat, entering a peripheral artery makes it possible to preserve the external carotid- and pterygopalatine artery (transected and ligated in intraluminal suture model). This approach is advantageous, as ischemic injury to mastication- and hypopharyngeal musculature with impaired mastication and swallowing is avoided, improving the nutritional status of the animal and thereby facilitating behavioural testing as an experimental read-out (Dittmar 2003; Shimamura et al.

2009). In the initial attempts to apply X-Ray fluoroscopy to direct a filament to the circle of Willis in rats, hemorrhage rates and variability in stroke volume were reduced (F. Sun et al. 2005). However, in these studies, the filament was, as in intraluminal suture model, placed in the circle of Willis, causing obstruction of the ACA and PComA and rendering large infarctions resembling malignant human infarction (Divani et al. 2015; Shimamura et al. 2009; F. Sun et al. 2005). From a neurointerventional point of perspective, we hypothesized that the smallest commercially available microwire for neurointerventional procedures (0.007-inch diameter) would be suitable for further navigation in the cerebrovasculature, i.e. to an occluding position in the M2-segment of the MCA, while at the same time not causing significant reductions in perfusion of the ipsilateral ACA and PComA.

1.2.2 Selective injections to the ICA

As mentioned in the previous section, microwire navigation is a fundamental part of IR. In the clinical setting the microwire provides a means to place catheters at different positions within the vasculature. Catheters for clinical applications come in a wide array of sizes and designs, allowing different kinds of manoeuvers and procedures. While the expanding use of rodents as models for human disease has persuaded successful translation of human imaging modalities, i.e. CT, MRI and positron emission tomography (PET), from bedside to use in small animals (i.e. micro-CT, high-field MRI (HF-MRI) and micro-PET), IR and digital subtraction angiography (DSA) as a research tool for small animals have not been readily available to the scientific community. However, a few recent reports have called for an increased presence of interventional radiologists in animal research (Solomon 2005; Solomon & Silverman 2010; Buhalog et al. 2010). The obvious contributions by IR to research are methods to achieve high spatial and temporal resolution imaging when delivering drugs, cells and radiotracers, among others, into selected organs or certain regions of the vascular tree. In experimental stroke, selective arterial access to the cerebral vasculature provides an extra dimension in the administration of treatment, as intra-arterial injections to the ICA would in all probability increase the local concentration of therapeutics at the target site.

From a clinical perspective, intra-arterial clot retrieval by mechanical thrombectomy has recently been demonstrated to have a strong benefit in patients with ischemic stroke and large vessel occlusion (Berkhemer et al. 2015; Goyal et al. 2015; Saver et al. 2015; Campbell et al. 2013). Mechanical thrombectomy involves placement of catheters in arteries supplying the brain regions affected by ischemia. The procedure therefore opens up the possibility to perform selective injections of treatment immediately after clot retrieval. Therefore, we decided to extend the MCAO model presented in this thesis to also include a method for brain-selective intra-arterial injections, a comprehensive experimental bench for further development of intra-arterial treatment performed back-to-back with clot retrieval.

1.3 MAGNETIC RESONANCE IMAGING

MRI has become an important tool in clinical and preclinical research. MR-scanners exist in parallel in the clinical and preclinical settings, a situation which to a large extent enables translation of research from bench to bedside and back again. In biomedical research, MRI enables non-invasive longitudinal assessment of brain morphology, physiology, function and metabolism at a relatively high temporal and spatial resolution.

In short, MRI of humans and animals employs the abundance of hydrogen in the body, mainly as part of water and fat. Atomic nuclei with an odd number of protons and/or neutrons, such as hydrogen (a proton), rotate about their axis, which makes them behave like magnets. When such nuclei are exposed to a strong magnetic field (B_0) like that created by a MR-scanner, they align parallel to B_0 and precess (i.e. rotate about their own axis, which in turn rotates about the direction of B_0). Precession occurs with a specific frequency (the Larmor resonance frequency) determined by the gyromagnetic ratio of the nucleus and the strength of the magnetic field. By further organizing the precessing protons by applying additional magnetic fields superimposed on B_0, the magnetic strength applied to different points in space will be different. This causes different resonance frequencies in protons in different regions of the object. The superimposed magnetic fields (magnetic field gradients) influence frequency and phase properties of precession. By delivering radiofrequency (RF) pulses with frequencies corresponding to the resonance frequencies for each region and sorting them by their phase, it is then possible to assemble an image with 3 dimensions, from signals generated by RF waves emitted due to the phenomenon of magnetic resonance. The phenomenon of magnetic resonance causes the protons in B_0 to re-emit electromagnetic signals, which are sampled by the MR-scanner, when returning to equilibrium after being excited by RF pulses with the resonance frequency.

1.3.1 Imaging of T2- and T1 relaxation

In clinical everyday work, T2 and T1 are terms broadly used by physicians to discriminate between two common types of MR images, where "T2-weighted" imaging (T2WI) may broadly be said to show water content while "T1-weighted" imaging (T1WI) shows fat. In a narrower sense, T2 and T1 are time constants introduced by Felix Bloch in 1946 (Bloch 1946), accounting for processes that force the excited protons to equilibrium, i.e. relaxation.

Briefly, T1 is a time constant accounting for thermal perturbations, transferring the energy added to the protons by the exciting RF-pulse to the surrounding tissue. The main determinant of T1 is the efficiency of movement of molecules, which in turn correlates to molecular size. Medium-sized molecules such as fat are much more effective in dissipating this energy when compared to water. This difference in energy dissipation is exploited when generating T1WI.

T2 on the other hand, accounts mainly for local irregularities in the magnetic field caused by the constant and inevitable motion of tissue protons. For example, fat contains more protons than water and thus exerts a stronger local magnetic field. Furthermore, large molecules move

slower and thus stay in contact for a longer time. This sustains the variation in the local magnetic field. Lipids contain more protons, i.e. are more magnetic, and stay in contact with adjacent molecules for a longer time when compared to water and consequently fat has shorter T2 than water. Local magnetic field variations are exploited when generating T2WI. Of note is that T1WI and T2WI do not exclusively reflect T1- and T2 values. Configuration of MRI scanning protocols involves varying repetition time (TR) and echo time (TE) in order to receiving signal more or less affected by T1 and T2. Thus, pixel intensities in T1W- and T2W images account for both processes determining T1 and T2, albeit with different contributions from each, depending on the TR and TE.

1.3.2 T2- and T1 relaxation in ischemic stroke

T1WI and T2WI are generally not sensitive to early changes in cerebral ischemia. However, they are useful in evaluation of subacute and chronic stages of ischemic stroke, as increases in T1 and T2 are believed to reflect changes in total water content in ischemic tissue. Breakdown of the blood-brain barrier by disruption of tight junctions and basal lamina degradation leads to isoosmotic vasogenic edema, causing accumulation of water in the extracellular compartment. As water molecules in biological tissues move around more than larger molecules such as lipids in brain tissue, the vasogenic edema will decrease the local magnetic field variation and thus prolong T2 relaxation. This is reflected by a signal increase in T2WI. However, there are probably several other factors influencing T1 and T2 in ischemic tissues, such as flow effects, shifts in the relative amounts of oxy- and deoxyhemoglobin, and magnetization transfer phenomena (Calamante et al. 1999).

1.3.3 Diffusion-weighted imaging

Diffusion-weighted imaging (DWI) is a commonly used MRI sequence for early diagnosis of brain ischemia. Diffusion in DWI refers to the movement of water molecules in tissue, caused by random thermal motions. Diffusion can be detected and measured by MRI. The principle of DWI is that a water molecule can be tagged to its initial location in the tissue by a first arrangement of magnetic fields. If the water molecule stays in its initial location after a second arrangement of magnetic fields, the signal from this location remains unchanged whereas there is a signal loss if the water molecule moves away from its initial location.

In practice, this principle is realized by superimposing yet another magnetic field (a diffusion gradient) on B_0 and the magnetic field gradients. The diffusion gradient changes the phase of the protons in water molecules depending on where they are located. Next, water molecules are allowed to diffuse before an identical diffusion gradient is applied albeit inverted. Subsequently, the phase of water molecules that stay in place will be restored (less diffusion, more signal) whereas water molecules moving more freely will experience two different phase shifts from the first and second diffusion gradient and thus not restore their phase (more diffusion, less signal). The strength and timing of the diffusion gradients can be varied to enhance or lessen the effects of diffusion on the image. The so-called b-value reflects the configuration of the diffusion gradients, a higher b-value produces a stronger diffusion effect.

In summary, regions of the brain with fast rates of diffusion (e.g. cerebrospinal fluid) will appear darker than regions with slower rates of diffusion (e.g. grey matter).

Natural barriers formed by membranes and organelles determine the distribution and movement of water molecules in biological tissues. Other determinants of diffusion of water in biological tissues are permeability of membranes, cellularity of tissues, transport processes and adsorption to macromolecules. DWI cannot separate the intrinsic diffusion of water molecules from all incoherent motions within the tissue, i.e. capillary pseudo-diffusion and gross motion, hence the introduction of the term "apparent diffusion". DWI images are generated using T2WI and thus contain T2 contrast, also referred to as "T2-shine through", making it difficult to discriminate restricted diffusion caused by cellular swelling (acute infarction) from prolonged T2 caused by vasogenic edema (subacute and chronic infarction). Therefore it is convenient to calculate a parametric image, in which, each voxel represent a pure apparent diffusion coefficient (ADC) devoid of T2 contrast. This image is referred to as the "ADC map".

1.3.4 Diffusion-weighted imaging in ischemic stroke

Ischemic brain tissue has slower than normal diffusion. The biophysical mechanisms that cause this decrease in diffusion are not completely understood. The initial hypothesis for the reason behind restricted diffusion was put forward by Moseley in 1990 (Moseley et al. 1990) and remains the most cited and generally appreciated theory. Moseley's compartment shift hypothesis relies on the temporal relationship between cellular swelling (cytotoxic edema) and ADC decrease in acute cerebral ischemia, both happening very fast. Ischemic cells depleted of ATP lose the functionality of their trans-membrane ion pumps, causing a shift of the displacement of water from the extra- to the intracellular compartment. It is widely assumed that diffusion is faster in the extracellular compartment (EC) compared to the intracellular compartment (IC), due to the relatively low concentration of macromolecules in the EC. A shift from the EC to the IC will therefore cause the ADC to decrease. However, evidence of this hypothesis remains indirect. A compartment shift as the sole or main contributor to ADC decline is highly unlikely considering the following circumstances: In the normal brain 80% of total brain water resides in the IC and 20% in the EC; the compartment shift due to cell swelling has been estimated to cause a mere <10% shift of total water from the EC to the IC (Schuier & Hossmann 1980). Evidence shows that the ADC for the EC and IC in healthy tissue are roughly similar (Duong et al. 1998). Another hypothesis is that the influx of water to the IC causes a volume reduction in the EC, bringing cell membranes closer, i.e. increased tortuosity of the EC, restricting diffusion by 35% in the EC (Norris et al. 1994). However, as the contribution of the EC to the total water brain signal under cytotoxic edema is 10%, even a large decrease of ADC in this fraction would make a very small contribution to the average decrease in ADC. It is reasonable to believe that the acute water ADC changes in the ischemic brain are mainly caused by changes in the IC and that the diffusion restriction by increased tortuosity in the EC contributes little to the average ADC. More recently, it was proposed that cessation of energy-dependent motion of intracellular

contents is the predominant mechanism for the decrease of intracellular ADC and thus the main contributor to the overall ADC decrease in the ischemic lesion (Duong et al. 1998).

1.3.5 Arterial spin labeling

Arterial spin labeling (ASL) MRI is a method for measurement of flow using magnetically tagged protons in inflowing blood as a contrast agent. More specifically, blood water in the cervical arteries is exposed to an inversion RF pulse. The result is inversion of the net magnetization of the blood water that is about to flow into the cerebrovasculature. After a short period of time the magnetically tagged blood water will flow through the brain and interact with parenchymal water, more or less reducing the magnetization of the tissue depending on the regional cerebral blood flow. At this point, a T1W "tag-image" is acquired. This "tag-image" is then subtracted from a "control image" acquired with the same parameters although without tagging of inflowing blood water. The resulting image will thus reflect the cerebral blood flow in each voxel within the transit time.

Although introduced already in the early 1990's, ASL has remained a technique for research and has, due to certain limitations, failed translation to the clinic. One limitation in measuring CBF in ischemic tissues is that the blood transit time to this tissue is increased causing underestimation of CBF with ASL (Zaharchuk 2014). Another limitation is overestimation of CBF in previously ischemic tissues as vasogenic edema causes an increase in T1 (Zaharchuk 2014). However, there are several advantages to ASL in the experimental setting. As no contrast agent needs to be added, repeated assessments of perfusion of ischemic events can be performed with high temporal resolution with low susceptibility to ischemia-related blood-brain barrier deterioriation.

1.3.6 Arterial spin labeling in ischemic stroke

MCA occlusion will cause a heterogenous decrease in perfusion of the brain matter supplied by the MCA, with collateral perfusion as a significant factor. In a simplified view, three territories of decreased perfusion can be defined:

- A severely ischemic region rapidly succumbing to infarction.
- A peri-infarct (penumbral) region determined for infarction if not reperfused within a certain period of time.
- An oligemic region viable yet hypoperfused with slight impairment of function.

In ischemic stroke, the non-salvageable infarct core gradually expands at the expense of surrounding penumbral regions. It is unclear for how long these penumbral regions remain uninfarcted, although it is reasonable to believe that penumbral regions exist well beyond the therapeutic time-window for reperfusion therapy (Markus 2004). Thus, the main target for therapy in recent years has been the hypoperfused region adjacent to the infarct core. Although ASL has shortcomings in producing exact and detailed measurements of CBF, the method is able to discriminate between regions with severely affected perfusion and regions with moderately affected perfusion in the experimental setting (Calamante et al. 1999;

Lythgoe et al. 2000). However, the intraluminal suture model produces a large region with severely affected perfusion and a relatively small peri-infarct region (Calamante et al. 1999). This has made it difficult to study patophysiological changes in the peri-infarct region and limited the validity of neuroprotective strategies aimed at peri-infarct salvage.

The stroke model described in Paper I, was designed to increase the size of the peri-infarct region, while reducing the invasiveness and ischemic lesion size, in order to more accurately model the perfusion situation in ischemic stroke in humans. We hypothesized that a more delicate intervention in the circle of Willis would to a larger extent preserve collateral flow over the brain surface, as provided by the ACA and the PComA.

1.3.7 MR Spectroscopy

MR spectroscopy (MRS) allows *in vivo* measurement of various metabolites. The principle of MRS is that the resonance frequency for nuclei is different depending on what chemical environment that the resonating protons reside in. The effect of different chemical compounds on the MR signal is very small and expressed in parts per million of the resonant frequency. The differences is however large enough to enable MRS to identify molecular structures and their relative concentrations. The clinical applications of MRS is currently mainly used in the diagnosis of brain tumors, although plays a minor role in this context. One limiting factor is that MRS at magnetic field strengths of clinical scanners is insensitive and therefore, in order to gather enough signal, restricted to sampling spectra from relative large brain volumes. However, with the introduction of clinical scanners with higher field strength, MRS may become more valuable as a diagnostic tool. The high field strengths in experimental MRI give the opportunity to perform MRS with better signal to noise ratio and an increased spectral, spatial and temporal resolution. Of primary interest in ischemic stroke is the possibility to detect elevated levels of lactate as an indicator of anaerobic glycolysis (Sappey-Marinier et al. 1992). Furthermore, MRS is also able to detect N-acetyl aspartate, a highly abundant amino acid present primarily in neurons and used as a marker of neuron viability. The level of N-acetyl aspartate is reduced following cerebral infarction (Sappey-Marinier et al. 1992). Thus, MRS is a promising tool for further advancement in the understanding of the pathophysiology of brain tissue under metabolic stress caused by ischemia.

1.4 POSITRON EMISSION TOMOGRAPHY

PET is a tool to visualize molecular and biochemical processes in biological tissues. In short, a positron emitting radionuclide is incorporated into a molecule, i.e. a radiotracer. The radiotracer is injected into the subject and depending on the molecule and the properties of the subject, the radiotracer distributes and metabolizes within the subject. The positrons emitted by the decaying radionuclide, i.e. antiparticles of electrons, combines with electrons (annihilates) within a few millimeters of the radiotracer and result in the emission of two 511 keV gamma photons moving away from the site of annihilation at almost 180 degrees to each other. The simultaneous detections of gamma photons in two detector elements 180 degrees apart in multiple rings of detectors can then be used to approximate the location of the radioactive decay. Next, the recorded data is reconstructed to generate 3-dimensional distributions of radioactivity, which can be used for quantification. Also, the recorded data can be reconstructed in time frames to provide information on time-dependent changes in radioactivity concentrations in different tissues, i.e. dynamic images.

Fluorodeoxyglucose, [2-^{18}F]-2-Fluoro-2-deoxy-D-glucose ([^{18}F]FDG), is a radiotracer commonly used in medical imaging. It is a glucose analog with the positron-emitting radionuclide fluorine-18 incorporated at the 2' position in the glucose molecule. Like glucose, [^{18}F]FDG is actively transported from the blood into the brain by glucose transporters, where it is phosporylated in the first step of the glycolysis by intracellular enzymes (hexokinases) to form [^{18}F]FDG 6-phosphate. Unlike glucose 6-phospate, [^{18}F]FDG 6-phosphate cannot enter the subsequent steps in glycolysis. Thus, [^{18}F]FDG decay reflects the intracellular distribution of glucose in the brain.

1.5 Glucose metabolism in the ischemic brain

During ischemic stroke, reduction of perfusion results in a significant impairment of oxygen- and glucose supply, leading to cellular dysfunctions due to loss of adenosine triphosphate (Heiss 2011). It is well known from experimental and clinical observations that glucose metabolism in the ischemic core is severely depressed (Wise et al. 1983; Yuan et al. 2013), whereas several experimental studies on glucose metabolism in penumbral and oligemic regions have indicated local increases in glucose metabolism (Ginsberg et al. 1977; Yuan et al. 2013; Sako et al. 1985; Welsh et al. 1980; Choki et al. 1984; Komatsumoto et al. 1989; Kita et al. 1995; Nedergaard et al. 1986; Ginsberg et al. 1985). This ischemic hypermetabolism, also known as uncoupling of flow and metabolism, has also been observed in human acute ischemic stroke and also in post-asphyctic infants (Nasu et al. 2002; Blennow et al. 1995). However, the underlying mechanism leading to the increase in uptake of [^{18}F]FDG in regions undergoing infarction remains unclear. Initially, it was hypothesized that it was caused by anaerobic glycolysis compensating for loss of adenosine triphosphate (Kita et al. 1995). Later it has been suggested that an increased aerobic glycolysis was a more probable cause (Wise et al. 1983; Yuan et al. 2013). It should be observed, however, that there are certain inherent problems with estimations of glucose metabolism by [^{18}F]FDG PET, that may complicate the evaluation of glucose uptake in the ischemic brain. For

instance, [^{18}F]FDG uptake may not be entirely representative of glucose metabolism in the ischemic brain. Even if metabolism of [^{18}F]FDG is very similar to glucose metabolism in normal brain tissue, there are small differences in transportation and phosphorylation between these two, which can be measured and expressed as a ratio called the "lumped constant" (Phelps 1981). It has been reported that hypoperfusion may cause a significant increase in the lumped constant (Nakai et al. 1988), which would mean that the increased [^{18}F]FDG uptake in the ischemic although yet uninfarcted brain could in large part be explained by an increased affinity towards [^{18}F]FDG over glucose. However, further studies are necessary to verify whether a change in the lumped constant is a significant factor in experimental [^{18}F]FDG PET imaging of the ischemic brain in rodents.

[^{18}F]FDG PET is thus an interesting tool for investigating alterations in glucose metabolism in acute ischemic stroke, especially in penumbral and oligemic regions where further understanding of tissue state and fate would be helpful in the development of neuroprotective strategies, specifically in cases where brain metabolism is targeted to ameliorate infarct progression. Also, it is well known that ischemic stroke is followed by elevated levels of blood glucose and it has been suggested that systemic hyperglycemia could have detrimental effects on brain tissue (Bruno et al. 2004). Furthermore, infarct related elevations in blood glucose have been proposed as a therapeutic target, as higher levels of blood glucose during acute ischemic stroke have been linked to larger infarct volumes and an increased functional impairment (Stead et al. 2009). However, in a recent randomized trial, ischemic stroke patients receiving insulin treatment to normalize systemic hyperglycemia had poorer outcomes and larger infarct growths (Rosso et al. 2012). It may be that systemic hyperglycemia is necessary to support a pathophysiological defense mechanism involving an acceleration of glycolysis in neurons and/or glia. Whether this can be linked to an increased demand for glucose in the ischemic penumbra is speculative. Regardless, further preclinical studies are warranted in order to learn how to handle systemic- and cerebral changes in glucose metabolism in ischemic stroke.

As mentioned, the existing models of ischemic stroke in the rat unfortunately produce a relatively small region of oligemia. Consequently, the preconditions for further investigations of the hypermetabolism of glucose are suboptimal. As one of the primary goals in designing a new model of experimental stroke (Paper I), was to more closely model human stroke by preserving collateral flow with prerequisites for a smaller focal ischemic core and a relatively large penumbral/oligemic region. We hypothesized that the newly designed model would facilitate observations of metabolic changes in ischemic and penumbral regions with [^{18}F]FDG PET.

1.6 VEGF-B as a potential target in treatment of ischemic stroke

Vascular endothelial growth factors (VEGFs, including VEGF-A, VEGF-B and placental growth factor PlGF) are major regulators of blood vessel physiology. In experimental stroke, the role of VEGFs have been assessed in angiogenesis, atherosclerosis, cerebral edema, postischemic brain- and vessel repair and neuroprotection (Greenberg & Jin 2013). In experimental cerebral ischemia, VEGF-A is the most thoroughly studied. It has been shown that VEGF-A protein expression is increased within hours- and over days to weeks after MCAO, primarily in the penumbra, and localized to neurons astrocytes and endothelial cells (Kovacs et al. 1996; Lennmyr et al. 1998; Hayashi et al. 1997). As VEGF-A is clearly involved in the brain response to acute and chronic ischemia, it has been considered a potential target for neuroprotective intervention. However, VEGF-A was, along with its angiogenic properties, initially identified based on its profound effects on vascular permeability (Senger et al. 1983; Ferrara & Henzel 1989). As development of cerebral edema is a complicating factor in ischemic stroke, it was hypothesized that VEGF-A could worsen infarct progression by opening up the blood-brain barrier. This was indeed the case when administration of VEGF-A to rats within the first hour of MCAO caused an increase in infarct size by worsening cerebral edema (Zhang et al. 2000). This has been further corroborated by studies showing that administration of anti-VEGF-A antibodies counteracts increased vascular permeability in a rat model of stroke (Kimura et al. 2005). Thus, the therapeutic potential of VEGF-A in ischemic stroke seems to be limited by its potent actions on blood-brain barrier permeability leading to vasogenic edema.

VEGF-B on the other hand, despite being very similar to VEGF-A, is not a mediator of vascular permeability (Gaál et al. 2013). Whether VEGF-B has angiogenic activity is under debate due to inconsistent and controversial results. Although the biological functions of VEGF-B remain incompletely understood, the fact that it does not mediate vascular permeability and has been shown to exert activity in the endogenous response to cerebral ischemia makes it a potential therapeutical target in ischemic stroke. However, the role of VEGF-B activity in cerebral ischemia is yet to be determined. The current evidence is conflicting, as increased VEGF-B reactivity in the ischemic border zone 24 hours after MCA occlusion in mice has been reported, whereas reduced amounts of VEGF-B protein was detected following the same procedure in rats (Li et al. 2008; Guan et al. 2011).

The prevalence of type-2 diabetes, one of the most important risk factors for ischemic stroke, is rapidly increasing and contribute to the increasing stroke incidence in developed countries (Kissela et al. 2005; Medin et al. 2004; Kissela et al. 2012). In parallel with emerging studies on the potential role of VEGF-B in the ischemic brain, VEGF-B antagonism has been reported to restore insulin sensitivity and reduce lipid accumulation in muscle. Based on these findings, a promising strategy to treat type-2 diabetes based on these findings has been suggested (Hagberg et al. 2012; Hagberg et al. 2013; Hagberg et al. 2010).

As VEGF-B antagonism is a potential treatment for of one of the major risk factors for ischemic stroke, and further investigations on whether VEGF-B antagonism would affect

development of ischemic stroke are anticipated. Interestingly, it was found that pre-treatment with a monoclonal anti-VEGF-B antibody ameliorated the ischemic injury in a photothrombotic mouse model (Nilsson & Su 2015). We investigated whether their observations from neutralizing VEGF-B in mice subjected to ischemic stroke, could be extended and confirmed in the model developed in Paper I by using the imaging protocols established in Paper III.

2 AIMS OF THE THESIS

The general aim of the present work was to establish a clinically relevant experimental platform for multimodal imaging investigations of treatment studies of cerebral ischemia. The platform would the make results from studies on pathophysiology and treatments rapidly translated to clinical practice.

The specific aims of each paper were:

Paper I: To develop a model for ischemic stroke in the rat that, compared to previously existing models, more closely resembles the majority of human stroke.

Paper II: To extend the methods developed in Paper I to include super-selective intra-arterial injections to the rat brain and to investigate infusate distribution following such injections.

Paper III: To assess changes in cerebral blood flow and glucose metabolism in rats with ischemic stroke secondary to the model developed in Paper I.

Paper IV: To study the effects of VEGF-B antagonism on ischemic lesion volume, cerebral blood flow and glucose metabolism, under experimental conditions developed in papers I and III.

3 METHODS

3.1 ANIMALS AND ETHICAL CONSIDERATIONS (PAPER I THROUGH IV)

All animal work was conducted in accordance with the Swedish Animal Welfare Board at Karolinska Institutet and approved by the the regional ethical committee. In all experiments, male Sprague-Dawley rats (350-450 g, Scanbur, Sollentuna, Sweden) were used. We chose Sprague-Dawley rats, as MCAO in these animals result in relatively moderate and consistent infarct sizes compared to Wistar-Kyoto, Fischer-344 and spontaneously hypertensive rats, which respond to MCAO with larger or more inconsistent infarcts (Ginsberg & Busto 1989). All experiments were performed using isoflurane inhalation anesthesia (ISO). Anesthesia was induced using 4% ISO mixed with 96% oxygen and subsequently maintained at 2% isoflurane. We chose ISO over injection anesthesia to minimize animal handling, for ease of control, larger safety margins and quicker recovery times. A potential disadvantage with ISO are its effects on infarct volume, CBF and VEGF expression (Taheri et al. 2014).

The stroke model presented in Paper I and II and used in Paper III and IV has several advantages over conventional MCAO models that are mutually attractive from scientific and ethical standpoints. In the widely used intraluminal suture occlusion model, a dissection of the neck is performed with ligation of the ECA. This causes ischemic necrosis of mastication and hypopharyngeal muscles with negative effects on animal well-being and outcome in behavioural testing (Dittmar 2003). Further, the intraluminal suture occlusion model causes a large and highly variable ischemic injury leaving some animals in severe neurological conditions, negatively impacting on modeling of treatable human stroke and animal well-being and has a relatively high hemorrhage rate. Using X-Ray fluoroscopy guidance, we were able to replace neck dissection with a small incision on the tail and furthermore by replacing crude filaments with microwires designed for endovascular neuronavigation, we were thus able to avoid undesired ischemic injury. In addition, our analysis of ischemic injury was mainly performed by non-invasive *in-vivo* imaging. *In-vivo* imaging allows repeated observations in the same animal, which consequently reduces the number of animals needed. In summary, the animal work in this thesis relies heavily on the use of advanced techniques that are non-invasive or minimally invasive with considerable positive effects on animal well-being. Two of the three components of the 3R principle, i.e. Reduction and Refinement are thus fulfilled using the current techniques. Replacement of animal models for studies on stroke is not yet possible due to the complexity of the CNS and the neurovascular unit and the necessity of having an existing circulation in order to mimic the human situation.

3.2 OCCLUSION OF THE MIDDLE CEREBRAL ARTERY (PAPER I, III AND IV)

In Paper I we developed a novel method for occluding the MCA in the rat by fluoroscopy-guided microwire navigation from the ventral tail artery to two different positions in the MCA of the rat. Furthermore, we demonstrated the possibility to occlude and reperfuse the MCA with the animal located inside an HF-MRI (9.4T) system. In Paper III, the developed method was used as a model for ischemic stroke in *in-vivo* imaging assessment of glucose uptake, lactate formation and cerebral blood flow. In Paper IV the model was used to assess the effect of VEGF-B antagonism on ischemic stroke.

Briefly, a midline incision was made on the ventral side of the tail. The fascia covering the ventral artery was cut, and the exposed artery was ligated distally. Next, a ligature was tied loosely around the proximal part of the artery, and a microvascular clip was placed over the ventral artery. The artery was cut and a hydrophilic microcatheter carrying a microwire was introduced and advanced to the thoracic aorta. We did choose the ventral tail artery over femoral arterial access to minimize the risk for peripheral ischemia, for minimal invasiveness and to shorten surgical exposure time.

Subsequent steps were performed using a Philips Allura FD20 interventional x-ray system (Philips Healthcare, The Netherlands). Two different interventional approaches were used 1) The microcatheter was advanced on a 0.18 mm microwire to the thoracic aorta, Next, the microwire was navigated to a tip position distal to the bifurcation of the MCA (Fig. 1a and 1b). 2) The microcatheter was advanced on a 0.25 mm microwire to the thoracic aorta. Next, the tip of the microwire was navigated into the MCA with the tip between the optic tract and the inferior cerebral vein (Fig. 1c and 1d). This position was maintained for 90 min in all animals. Thereafter the microwire was retracted together with the microcatheter out of the animal and the proximal ligature on the tail artery was tightened and the incision was closed.

The choice of dimensions for the occluding microwires were made based on the known approximate diameter of the MCA in rats - 0.24 mm (Scremin 1995). Hence, we hypothesized that a 0.18 mm microwire could be placed with the tip occluding the MCA distal to where the vessel traverses the rhinal fissure, albeit without occluding the lateral and lenticulostriate end arteries originating proximal to where the MCA traverses the olfactory tract. A 0.25 mm microwire placed with the tip at the position approximate to the olfactory tract would instead occlude the M1 segment of the MCA and also lateral lenticulostriate end arteries.

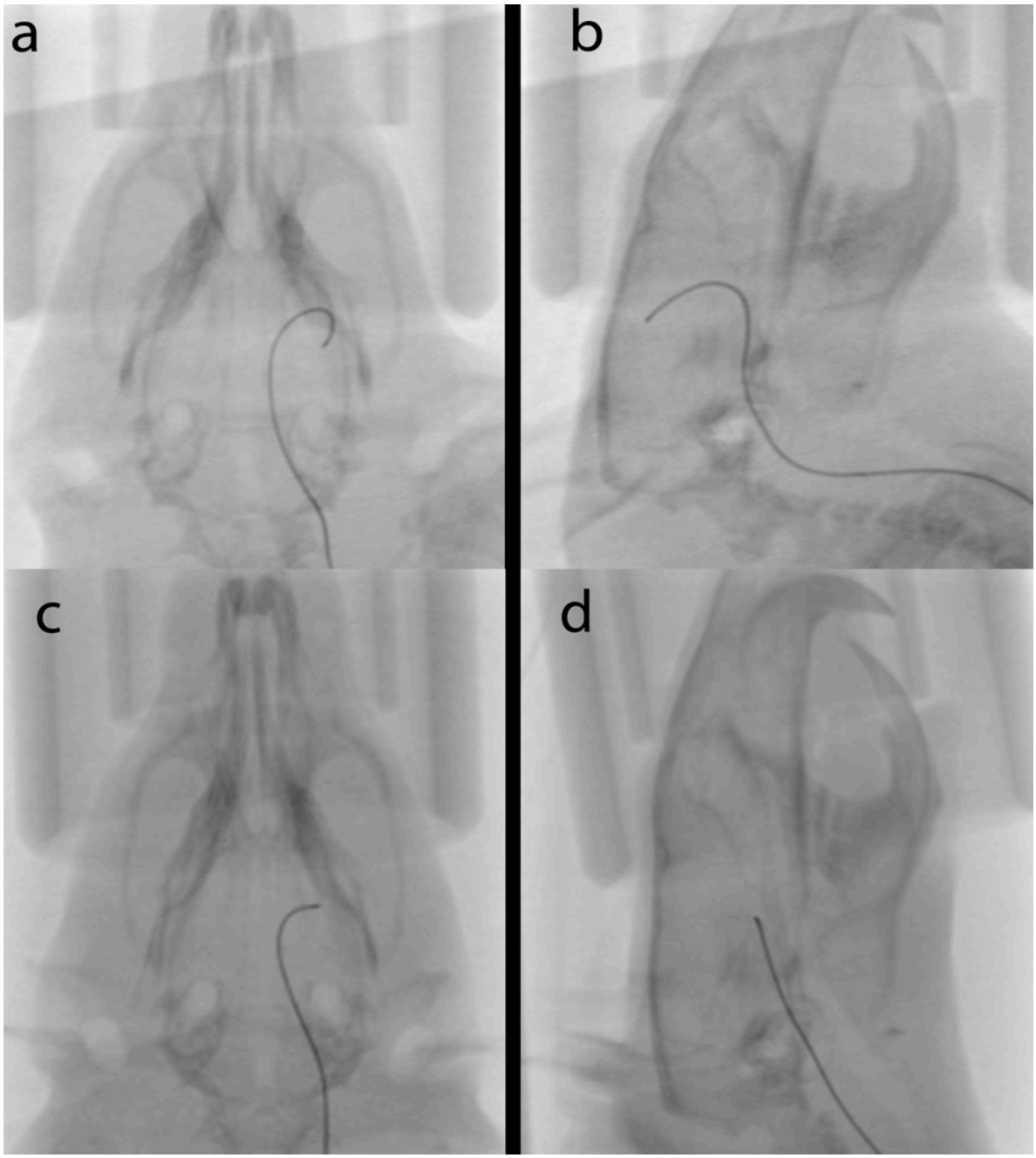

Fig. 1. Radiographic images showing microwire placement in different segments of the middle cerebral artery (MCA) in the rat. (**a** and **b**) Axial and sagittal projections of microwire placement in the M2 segment of the MCA. (**c** and **d**) Axial and sagittal projections of microwire placement in the M1 segment of the MCA.

3.3 SELECTIVE INJECTIONS TO CERVICAL ARTERIES (PAPER II)

In Paper II we extended the endovascular procedures developed in Paper I to include navigation of microcatheters to different segments of the carotid artery with subsequent injection of iodine contrast media and [^{18}F]FDG.

The ventral tail artery was used for arterial access. We navigated the microcatheter to three different positions: 1) in the common carotid artery (CCA) (Fig 2A and 2B), 2) in the cervical internal carotid (cICA) although proximal to the branching of the pterygopalatine artery (PPA), 3) distal to the PPA in the intracranial part of the internal carotid artery (iICA) (Fig 2C and 2D). In these positions, we performed DSA by injections of 100 μL Iohexol (Omnipaque; Amersham Health; 180mg/ml of iodine) (Fig 2A and 2C) and injections of [^{18}F]FDG (10-20 MBq, 500 μL) followed by a saline flush of 300 μL, injected in each animal at a rate of 0.125 ml/min (Fig. 2B and D). The choice of two injection sites in the ICA was determined by the consistent PPA anatomy found in rats. The PPA, an inconsistent rudimentary vessel in humans, is of comparable size to the ICA in rats. The PPA supplies mostly extracranial tissue with the exception for the middle meningeal artery. Due to its size, we hypothesized that a brain-selective injection would have to be performed distal to the origin of the PPA. As the diameter of the ICA in rats is approximately 0.7 mm (Scremin 1995) we used the smallest commercially available navigable catheter for intervention (outer diameter 0.44 mm) to minimize the risk for occluding the vessel.

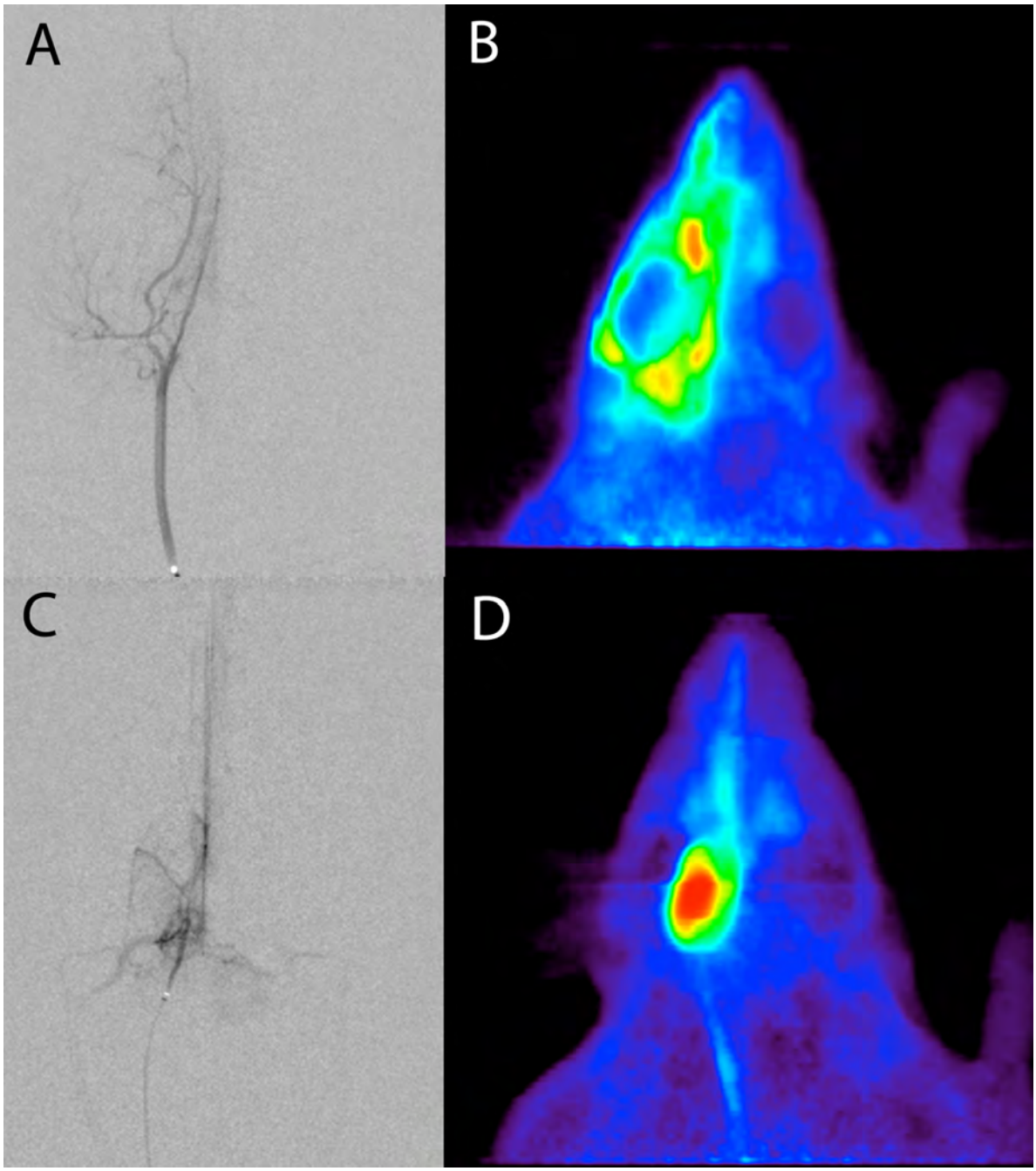

Fig. 2. Digital subtraction angiography (DSA) and PET in the rat, following intra-arterial injections of Iohexol and [^{18}F]FDG. (**A** and **B**) Injection into the common carotid artery. (**C** and **D**) Injection into the internal carotid artery, distal to the origin of the pterygopalatine artery.

3.4 MR IMAGING (PAPER I, III AND IV)

The MRI experiments were conducted using a horizontal 9.4 T magnet (Varian, Yarnton, UK) equipped with a 12 cm inner diameter gradient system with maximum gradient strength of 600 mT/m. A 72 mm birdcage volume coil was used for excitation (Rapid Biomedical GmbH, Würzburg-Rimpar, Germany) and a 4-channel phased array surface coil (Rapid Biomedical GmbH, Würzburg-Rimpar, Germany), designed for imaging of the rat brain, served as receiving coil. Due to the proximity of the interventional X-ray system and the MR-scanner it was possible to transfer the animal to the MRI within 5 minutes after occluding the MCA. Temperature was maintained at 37 ± 0.5 ºC throughout the MRI experiment with a feedback controlled air-heater system (SA-Instruments, Inc, Stony Brook, NY, USA). The pulse, oxygen saturation and respiration rate was monitored using an MR-compatible system (SA-Instruments, Inc, Stony Brook, NY, USA).

3.4.1 T2WI

In the development of the M2CAO (Paper I), we were interested in acquiring images with high anatomical resolution and sensitivity for ischemia in order to characterize the injury. Therefore, we obtained 3D volumetric data of the entire brain using a fast spin-echo 3D pulse sequence resulting in mainly T2-weighted images (TR 1000 ms, effective TE 58.7 ms, ETL 4, data matrix (RO x PE x PE2) 1024 x 128 x 128, covering a field of view (FOV) of 51.2 x 22.0 x 19.2 mm^3 in the tail-head, left-right and ventral-dorsal, directions respectively. Excitation of the spins was accomplished by a 1.61 ms sinc pulse while 1.29 ms sinc pulses were used for refocusing, spectral width 100 kHz, and one average was used, resulting in a scan time of 1h 4 min. Signals outside field of view (FOV) was suppressed with three spatial saturation bands positioned lateral and ventral of the brain. The saturation bands slightly overlapped with the FOV.

In Paper III and IV, we employed a simpler approach to generate T2WI to shorten time in order to accommodate more time-consuming image sequences. We simply used the T2 image obtained in the DWI sequence when diffusion gradients are set to zero (b = 0). By doing this we also had the advantage of T2WI and DWI images of same size and therefore co-registration was facilitated.

3.4.2 Diffusion-weighted imaging

When performing MR experiments for Paper I, we were limited to somewhat rudimentary DWI as the scanner had been newly installed and image sequences were yet to be implemented and developed.

In Paper I, ADC-maps were estimated from diffusion weighted multi-slice spin-echo echo planar imaging (EPI) data. 18 continuous coronary slices of 1 mm thickness were acquired with a FOV of 38 x 19 mm^2 and a matrix of 128 x 64 in the horizontal read out and vertical phase encode directions, respectively. A long TR of 10 s was used to avoid systematic errors due to incomplete relaxation between reference scans and diffusion weighted scans, while

effective TE was 50 ms. Diffusion weighting was accomplished through gradient pulses of 2.2 ms and amplitude of 584.9 mT/m applied along the RO-direction applied before and after the refocusing pulse. The diffusion encoding and decoding gradient pulses were separated by 10 ms to yield a target b-value of 1100 s/mm^2. Reference images, without diffusion weighting were acquired with the amplitude of the diffusion encoding gradients set to zero.

For Paper III and IV, we were able to apply a more comprehensive pulse sequence for diffusion tensor imaging, using multi-slice three-shot spin-echo EPI sequence in transverse plane (14 slices of 1mm thickness) with repetition time (TR) 3 s, echo time (TE) 25 ms, field of view 32 × 32 mm^2, matrix size 96 × 96, in-plane resolution of 33 × 33 μm, diffusion gradient duration (Δ) 2.3 ms and diffusion gradient separation (δ) 6.5 ms. Diffusion sensitizing gradients were applied along 12 directions with two diffusion sensitizing factors b = 0 and 1000 s/mm^2.

3.4.3 Arterial spin labeling (Paper III and IV)

For perfusion measurements, an arterial spin labeling surface coil (Rapid Biomedical GmbH) was placed 2 cm away from the head coil underneath the neck.

Perfusion measurements were performed using three-shot gradient EPI with a FOV of 32 × 32 mm^2, matrix size 96 × 96, TR 6.15 s, TE 10.5 ms and 14 slices of 1 mm thickness with no gap in between. Continuous arterial spin labeling was accomplished by applying an off-resonance RF power to the ASL coil in the presence of a 1 Gauss/cm gradient during TR. The labelling plane was located 2.4 cm upstream from the imaging slice package and a transit time (TI) of 2 ms was assigned to the labelled blood moving away from the tagging plane. A pair of tagged and control images were acquired for each slice. To acquire the control image, the tag position was reversed by switching the sign of the labelling offset-frequency, resulting in the tagging plane being moved downstream to the imaging plane.

3.4.4 Spectroscopy Paper (III)

^{1}H MRI spectra were acquired using point resolved spectroscopy (PRESS) sequence from a volume of interest (VOI) (2.5×1.7×2.5 mm^3). Two separate VOIs were placed, one in the infarct core showing restricted diffusion and another in the peri-infarct region. The water suppressed spectrum was acquired with TR 3 s, a total TE 15.66 ms, 3 ppm offset from water signal, spectral width 8013Hz, 4096 complex data points and 32 scans, with a total acquisition time of 1.42 min. The water signal was suppressed with variable power RF pulses and optimized relaxation delays (VAPOR). A water reference scan was recorded per each water-suppressed spectrum for quantification and eddy current compensation purposes. The gradient polarity was reversed to compensate for the chemical shift displacement artefacts due to spectral lipid contamination.

3.5 MRI DATA PROCESSING AND IMAGE ANALYSIS

All MRI data were initially processed with VnmrJ software (Agilent Technologies, Palo Alto, CA, USA) and imported to ImageJ software (National Institutes of Health, Maryland, USA)(Schneider et al. 2012). ImageJ data were either formatted for export to another software or processed directly according to descriptions in the next sections.

3.5.1 Assessment of infarct volume

In Paper I, volumetric T2 images were imported to OsiriX imaging software (OsiriX Foundation, Geneva, Switzerland). Volumes were built by manual tracing of the infarct defined by visual assessment as increased signal intensity. Manual tracing was performed in section intervals of 1 mm; the final volume was established through software interpolation and volume calculation. Two independent observers measured infarct volumes.

In Paper III and IV, segmentation of infarct volumes was performed in ITK-SNAP (Yushkevich et al. 2006). The reason for choosing ITK-SNAP over OsiriX imaging software was that ITK-SNAP is a software application dedicated to segment structures in 3D medical images and hence has a more efficient workflow for doing this.

3.5.2 CBF measurements

CBF maps were calculated from ASL images using ImageJ software (National Institutes of Health, Maryland, USA). Next, the CBF maps were imported together with ADC maps acquired back-to-back and co-registered in ITK-SNAP. Briefly, an ischemic region was manually segmented by visual determination of regions displaying restricted diffusion on ADC images and an oligemic region was determined by visually assessing regions adjacent to the ischemic region displaying perfusion deficit but not showing diffusion restriction.

3.6 PET (Paper II, III and IV)

The PET investigations were performed on a MicroPET Focus 120 (CTI Concorde Microsystems) with a spatial resolution of 1.3 mm. The [^{18}F]FDG used was obtained from daily productions for clinical PET at the Karolinska University Hospital and had passed all quality requirements for administrations in humans. During scans, animals were kept normothermic on a heating pad.

In Paper II and III, dynamic series of PET images were created to characterize spatiotemporal glucose uptake patterns. In Paper II, we investigated the dynamics of [^{18}F]FDG following intra-arterial injection with varying degree of brain selectivity. In Paper III we assessed spatiotemporal [^{18}F]FDG uptake patterns in relation to cerebral ischemia. Also, by creating dynamic imaging series, we were able to apply compartmental quantification methods to estimate intracellular trapping of [^{18}F]FDG. Based on our findings in Paper III, we were in Paper IV able to tailor an imaging protocol specifically aimed at assessment of the time period following M2CAO when the hypoxy-related increased uptake in [^{18}F]FDG uptake is readily detectable and this way limit necessary scan time.

In Paper II, animals were catheterized under fluoroscopic guidance as described above. Next, they were moved to the MicroPET with the head in the field of view. [^{18}F]FDG was injected intra-arterially as described above. One group of animals received intravenous injection only. After injection, data were collected continuously for 25 minutes.

In Paper III, animals were placed in the PET scanner with the head in the field of view within five min after placement of the microwire in the MCA. [^{18}F]FDG was administered via the tail vein (20-40 MBq, 500 μL). Data were collected continuously during 90 min from the time of injection. Next, the microwire was retracted and a second injection of [^{18}F]FDG was administered via the tail vein (20-40 MBq, 500 μL) followed by data collection during 60 min from the time of reperfusion. One group of animals were placed in the PET scanner 24 h after reperfusion, followed by [^{18}F]FDG administration via the tail vein (20-40 MBq, 500 μL) and data collection during 60 min.

In Paper IV, animals were subjected to M2CAO and [^{18}F]FDG was administered via the tail vein (20-40 MBq, 500 μL) within 10 minutes after placement of the microwire in the MCA. Animals were placed in the PET scanner with the head in the field of view and data were collected continuously over the last 20 minutes of the 90 minutes occlusion time. Additional PET scans at baseline and at 7 days after M2CAO were performed in the same fashion, albeit without M2CAO, i.e. [^{18}F]FDG was administered via the tail vein followed by 20 minutes of data collection after 60 minutes.

3.6.1 PET data processing and image analysis

PET data were processed with MicroPET manager and evaluated using the Inveon Research Workplace (Siemens Medical Solutions) software. All imaging data were corrected for radioactive decay, random coincidences (photons from different annihilations detected at the same time), scattered photons (photons changing direction in tissue and detected), and detector dead time (the time when the detector is saturated by photon coincidences and unable to register new coincidences). Image data were not corrected for attenuation. In small-animal imaging of the brain, the impact of attenuation is very small, compared to human PET, as the amount of attenuating tissue is much smaller.

In Paper II, volumes of interest (VOI) were manually drawn over hemispheres to create time-activity curves from each VOI). In Paper III and IV, MRI from 24 hours after M2CAO was co-registered with PET registration of M2CAO and immediately after reperfusion. VOIs were manually drawn on the PET image using the co-registered CBF- and ADC-maps to create time-activity curves for [^{18}F]FDG uptake in the ischemic region succumbing to infarction and peri-infarct regions.

3.7 EX-VIVO ANALYSIS (PAPER III)

Even if MRI is highly sensitive in detecting brain infarction, more detailed information on the viability status of brain regions showing diffusion restriction and/or perfusion deficit and/or increased [^{18}F]FDG uptake can only be achieved by ex-vivo techniques.

In this thesis we further validated the apparent MRI and PET lesions by 2,3,5-triphenyltetrazolium chloride (TTC) staining. Immediately after sacrifice coronal 2 mm sections were taken throughout the brain and immersed in a 2% solution of 2,3,5-triphenyltetrazolium chloride (TTC) in normal saline at 37°C for 30 min, after which the sections were fixed in 10% phosphate buffered formalin for photography. TTC is a cheap and fast technique that provides macroscopic differentiation between viable tissues from infarction (Liu et al. 2009). TTC is colourless until reduced to a red stain by dehydrogenases in functionally intact mitochondria. Although there are discussions on the sensitivity of this technique, it is regarded as highly specific (Liu et al. 2009).

To investigate apparent MRI and PET lesions on a microscopic level, we applied immunohistochemistry (IHC) in Paper III to further examine cellular viability and also blood-brain barrier integrity. The brains from animals in groups were removed immediately after sacrifice by decapitation and snap frozen in isopentane-dry ice. Coronal 14 μm cryosections were taken at -15°C throughout the infarct and peri-infarct regions using a Leica cryostat (CM3000, Leica Instruments GmbH, Nussloch, Germany). The sections were thaw mounted and stored at -20°C prior to use.

To visualize apoptotic staining, the ApopTag Fluorescein Detection kits (EMD Millipore, Billerica, Massachusetts, USA) were used. The apoTag kit relies on Terminal deoxynucleotidyl transferase dUTP Nick End Labelling (TUNEL) staining. Briefly, sections were placed in fresh 4% paraformaldehyde solution, post-fixed in ethanol:acetic acid solution and incubated in TdT solution for one hour at 37^{o}C. Stop/wash buffer was added and the slides were finally incubated with Anti-Digoxigenin Conjugate solution for 30min. In addition to staining for apoptosis the same slides were also stained with antibodies against Rat IgG to detect opening of the blood-brain barrier. Briefly, sections were washed in Tris-HCl buffered saline (pH 7.4) and incubated in blocking buffer containing anti-rat secondary antibodies (1/200, Jackson) followed by several washes in Tris-HCl buffered saline containing 0.5% tween. All sections were counterstained with the nuclear marker Hoechst (1/5,000) and mounted with polyvinyl alcohol/glycerol containing 2.5% DABCO (Sigma). To further assess blood-brain barrier integrity, fluorescein isothiocyanate (FITC)-dextran (4kDa, Sigma-Aldrich; 500 ml of 50mg/ml) in phosphate-buffered saline was injected via the tail vein immediately after reperfusion and after 24h after reperfusion. The animals were sacrificed 15 min after the injection.

3.8 STATISTICAL ANALYSIS (PAPER I THROUGH IV)

In Paper I a non-parametrical test (Mann-Whitney) was used to compare two groups. In Paper II a parametrical test (ANOVA) was used to compare three groups, assuming equal variances. In Paper III, a matched-pairs non-parametric test (Wilcoxon) was used to assess differences between hemispheres. In Paper III the Mann-Whitney test was applied when analysing differences between treatment groups and the Wilcoxon test was applied when analysing differences in the same animal at different time points. The reason for choosing non-parametric tests over their parametric counterparts in Paper I, III and IV, was that data appeared non-normally distributed and that the number of animals did not not meet the sample size guidelines for performing parametric tests on non-normally distributed data. Furthermore, the distribution of infarct volumes appeared skewed and therefore would the centre of the distribution be better measured by the median instead of the mean.

4 RESULTS AND DISCUSSION

In this thesis clinical endovascular techniques were translated into research tools for modelling of focal, ischemic stroke in the rat and into methods for intra-arterial access to the rat brain. Multimodal imaging was applied to characterize tissue infarction, metabolism and blood flow caused by the presented model for ischemic stroke. Finally, the model was applied in a treatment study, in which multimodality imaging was used to study the effects of VEGF-B antagonism.

4.1 A NEW RAT MODEL FOR ISCHEMIC STROKE (PAPER I)

In this paper we introduced a fluoroscopy-guided technique for microcatheter navigation from the medial tail artery to two different occluding positions in the MCA. We compared the ischemic lesions produced by these two occluding positions with regard to anatomical localization and volume. Also, we demonstrated the possibility to occlude and reperfuse the MCA with the rat located inside a high field (9.4T) MR-scanner.

In preliminary studies to Paper I, we found that it was feasible to use X-ray fluoroscopy guidance to navigate the smallest available clinical routine microwires (0.18 and 0.24 mm) from the ventral tail artery to different positions in the middle cerebral artery in Sprague Dawley rats weighing between 350-450g. Initially, we relied on angiography to visualize the arterial vessels for navigation. As angiography requires injections of iodine contrast media with extraction and insertion of the microwire, we abandoned this procedure when we realized that knowledge of vascular anatomy in relation to skeletal landmarks properly projected by fluoroscopy were sufficient for exact navigation during a short time span.

When the navigation procedure had been established, we tested the hypothesis that placement of microwires of different diameters at different locations in the MCA would produce either focal cortical infarction or subcortical infarction. Results confirmed that placement of a 0.18 mm microwire in the M2 segment of the MCA produced focal cortical infarcts in 13 out of 13 animals, although not exclusively as subcortical infarcts were detected in 4 of the animals (Fig. 3A and 3C). Importantly, no ischemic injury was detected in hypothalamic regions. Placement of a 0.24 mm microwire in the M1 segment of the MCA resulted in striatal infarction in 5 out of 5 animals with cortical infarcts in 2 out of 5 (Fig. 3B).

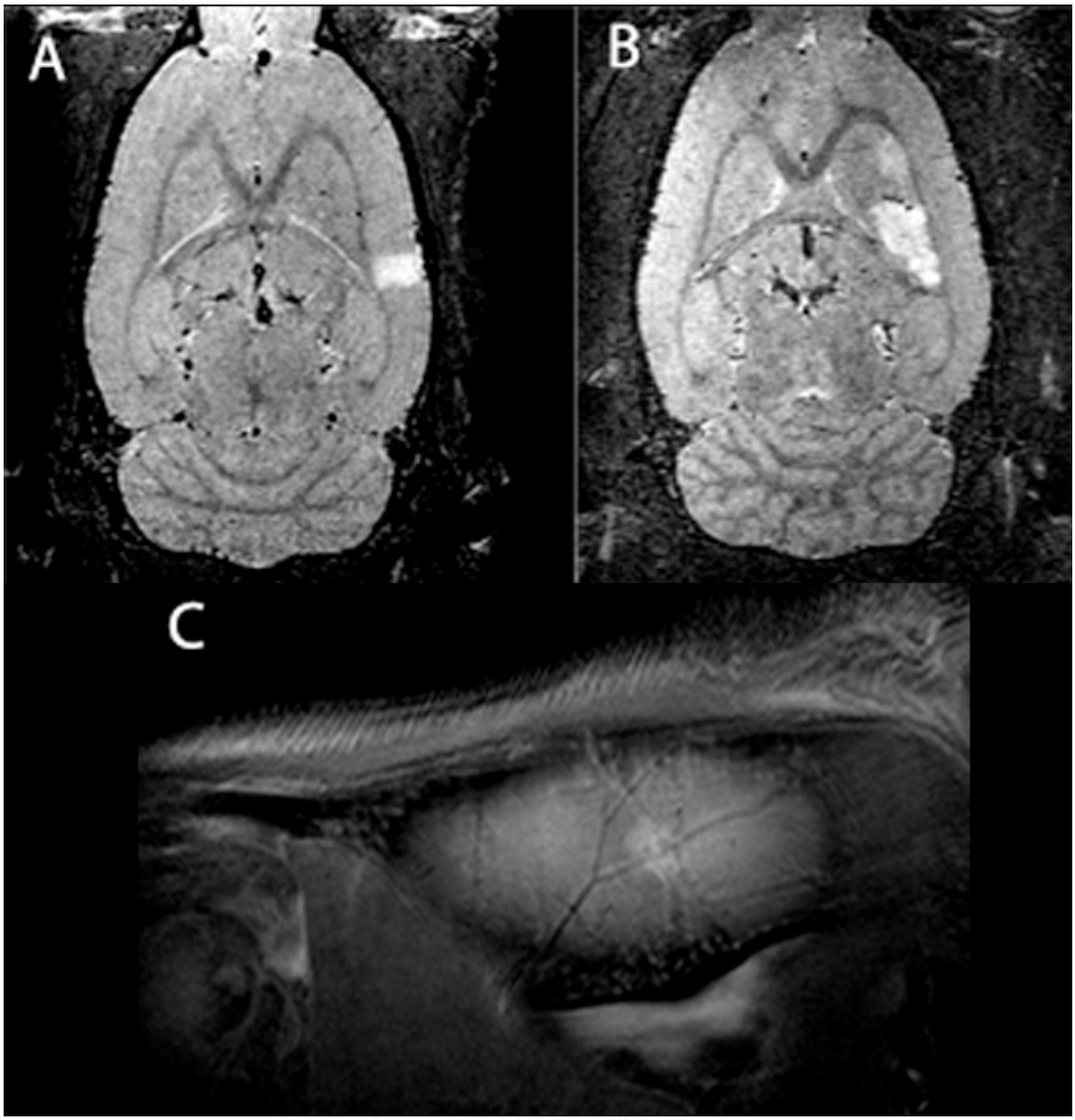

Fig. 3. T2-weighted HF-MRI showing infarct lesions in the rat. (**A**) Axial image showing a cortical lesion produced by microwire placement in the M2 segment of the middle cerebral artery (MCA). (**B**) Axial image showing a subcortical lesion produced by microwire placement in the M1 segment of the MCA **(C)** Sagittal image exhibiting the standard branching pattern of the MCA with infarction of temporal cortex supplied by a posterior branch of the MCA.

Another hypothesis was that placing of a 0.18 mm microwire in the M2 segment of the MCA would produce an infarct of smaller size than the intraluminal suture model, thus more closely modelling average human strokes instead of malignant infarction. The intraluminal suture model on average renders infarction of approximately 30% of the cerebral hemisphere, i.e. infarct sizes averaging 100 mm^3 (Carmichael 2005). The mean infarct volume produced by M2CAO was 23 mm^3, corresponding to infarction of 8 % of the hemisphere. In humans, strokes commonly range from 4.5 to 14% (Brott et al. 1989; Carmichael 2005). We concluded that one of the strengths of the M2CAO was indeed that infarct volumes produced would to better mimic those human infarctions where neuroprotective treatment would be applied first-hand. We hypothesized that the procedure would preserve collateral flow to a

large extent and cause a relatively large hypoperfused peri-infarct region, and that this situation would offer a greater possibility to study perilesional pathophysiology. This was indeed confirmed by the results from our investigations performed in Paper III. Moreover, we found the model to be highly compatible with in-bore studies using HF-MRI. We found that it was feasible to manipulate the microwire under MRI guidance. One question was obviously how much signal distortion would be caused by the microwire, made out of a nickel-titanium alloy (nitinol). Our findings showed that signal distortion was apparent, although very discrete, and did not interfere with assessment of infarct development using T2WI and DWI. This is explained in large part by nitinol being non-magnetic.

Another important aspect of modelling human ischemic stroke is the assessment of functional outcomes, especially in treatment studies. As the main outcome parameters in human stroke are long-term survival and functional recovery, measured by the Rankin scale or Barthel index, it is important that these outcomes are used also in the experimental situation (Mergenthaler & Meisel 2012). In the development of the model presented in Paper I, we hypothesized that we could apply a neurologic grading system developed by Bederson et al. to assess functional impairment (Bederson et al. 1986). This was however not the case, as the animals were found to have no observable deficit at 2, 4 and 24 hours after reperfusion. The explanation for this is simply that the infarcts were significantly smaller than the infarcts produced by the models used by Bederson et al. An important next step would be to design a functional grading system that is sensitive enough to differentiate degrees of improvement/deterioriation in function caused by infarcts produced through M2CAO in rats.

4.2 INTRA-ARTERIAL INJECTIONS TO THE RAT BRAIN (PAPER II)

In this study we extended the methods for microwire navigation under fluoroscopy developed in Paper I, to include navigation and positioning of commercially available microcatheters in the rat. The aim was to establish means to access the arterial supply of the rat brain in a minimally invasive and controlled manner, in order to accommodate injections of therapeutic and diagnostic agents. This is highly clinically relevant now since endovascular stroke treatment is rapidly being accepted as treatment for large vessel occlusions (Berkhemer et al. 2015; Goyal et al. 2015; Saver et al. 2015; Campbell et al. 2013; Molina et al. 2013). Mechanical thrombectomy includes positioning of microcatheters in the cerebral vessels and thus make it possible to inject therapeutic or diagnostic agents in a clinical situation. Paper II aims at developing a model for such intra-arterial injections in the rat. To assess distribution of the infusate, we analyzed radioligand uptake and iodine contrast distribution in the intra- and extracranial circulation of the rat, after intra-arterial injections to the common carotid artery and different parts of the internal carotid artery.

Beginning with injections to the CCA, we found that injections at a slow rate in the CCA or the proximal part of the ICA, before the origin of the pterygopalatine artery, resulted in streaming of the major part of the infusate to the extracranial circulation. This is readily explained by the carotid anatomy of the rat, where the CCA directs blood flow to the extracranial circulation to a larger extent than in man (Scremin 1995). In the rat, a significant

amount of the blood flow in the CCA is distributed to the ECA and the resulting blood flow in the ICA is divided between the PPA and the iICA.

In order to achieve a higher degree of exposure to the brain to our injections, we moved distally in the carotid artery and investigated the distribution of infusate when positioning the microcatheter tip distal to the ECA branching, although proximal to the PPA. However, injections of iodine contrast with this position resulted in reproducible opacification of the PPA whereas opacification of the iICA territory was intermittent and substantially weaker than the PPA. Thus, in order to achieve robust distribution of iodine contrast media and [^{18}F]FDG to the brain, the microcatheter had to be positioned in the iICA (Fig.4A and 4B).

In this study we also found that it is possible to enhance the uptake of [^{18}F]FDG by a factor of nine in the brain by intra-arterial injection and dramatically improve the contrast between brain and extracranial tissues. Superselective administration of a wide range of radioligands could markedly increase the sensitivity and resolution of nuclear medicine studies in diverse diagnostic and therapeutic approaches.

In summary, in Paper II we extend the methodology developed in Paper I, providing microcatheter access to the internal carotid artery along with the method of microwire occlusion of select segments of the MCA in the rat. We thereby provide a rat model for studies on superselective intra-arterial administration of therapeutic and diagnostic agents in the setting of ischemic stroke and other CNS diseases. Moreover, we demonstrate the advantages of selective intra-arterial injections by showing the differences in distribution of [^{18}F]FDG when administered with different degrees of selectivity. To reach the cerebral circulation efficiently in the rat, one needs to position the microcatheter distal to the origin of the PPA.

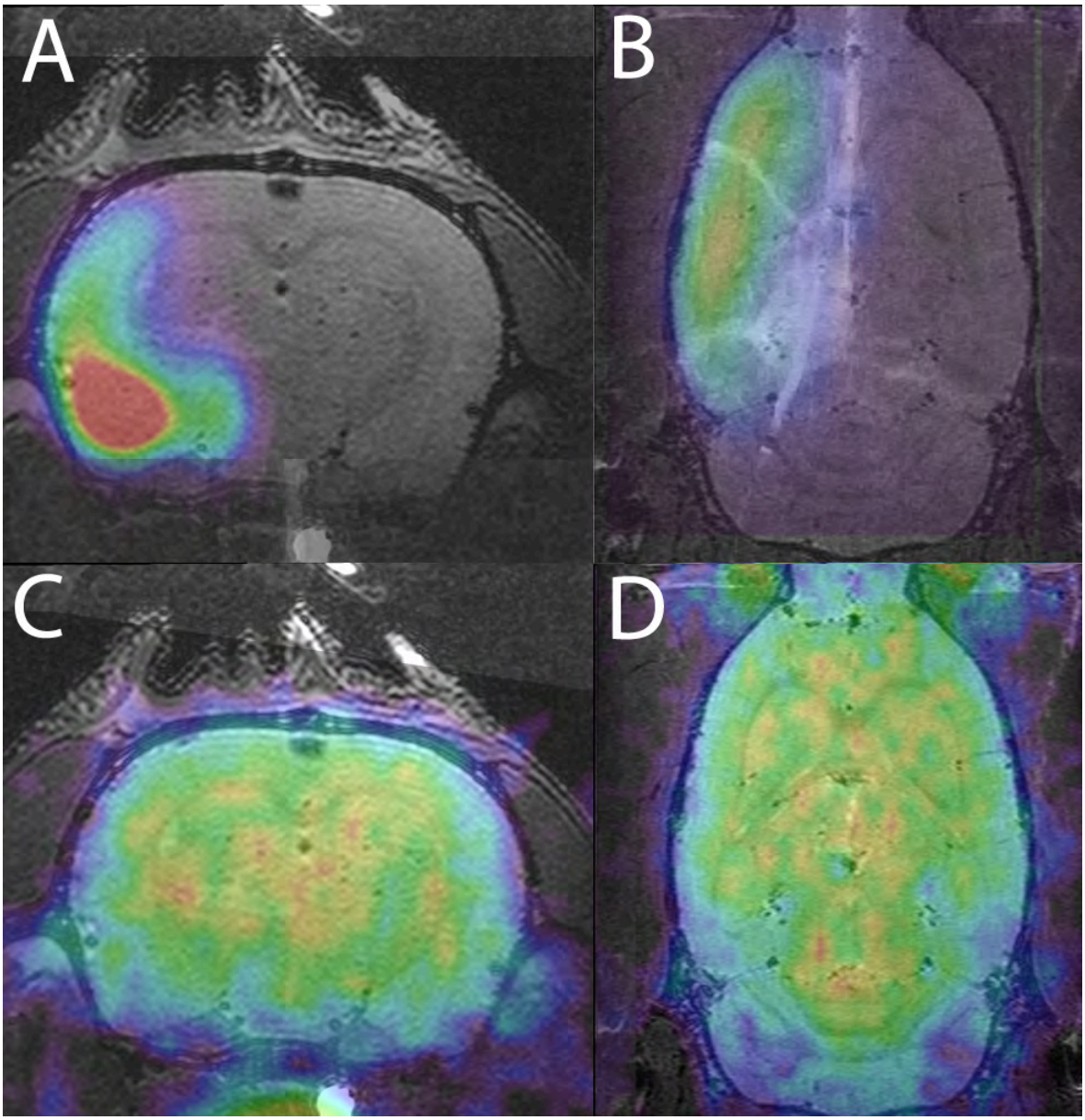

Fig. 4. [^{18}F]FDG PET images and digital subtraction angiography (DSA) co-registered with a HF-MRI template of the rat brain. (**A**) Coronal image of hemispheric [^{18}F]FDG uptake following intra-arterial injection to the internal carotid artery (ICA), distal to the branching of the pterygopalatine artery (PPA). (**B**) Axial image of hemispheric [^{18}F]FDG uptake following intra-arterial injection to the ICA, distal to the origin of the PPA, co-registration with DSA show an arteriogram of the circle of Willis (white). (**C** and **D)** [^{18}F]FDG uptake following intravenous injection.

4.3 IMAGING ISCHEMIC STROKE - METABOLISM AND BLOOD FLOW (PAPER III)

In Paper III we investigated regional dynamics of glucose metabolism in relation to cerebral blood flow, diffusion of water and immunohistochemical outcome, in the rat model of focal stroke developed in Paper I.

We found that PET imaging, following intravenous administration of [^{18}F]FDG, directly after occlusion of the M2 segment of the MCA, detected a markedly elevated [^{18}F]FDG uptake within the targeted MCA territory (Fig. 5B). This itself was not surprising, as the phenomenon of glucose hypermetabolism in acute brain ischemia has been thoroughly reported (Sako et al. 1985; Welsh et al. 1980; Choki et al. 1984; Komatsumoto et al. 1989; Kita et al. 1995; Nedergaard et al. 1986; Ginsberg et al. 1985; Belayev et al. 1997; Carmichael et al. 2004; Yuan et al. 2013). The distribution of the hypermetabolic regions demonstrated in this paper was significantly different in comparison with recent [^{18}F]FDG-PET investigations of acute experimental stroke. The first study by Yuan et al., in which Long-Evans rats were subjected to the intraluminal suture model (Belayev et al. 1996), [^{18}F]FDG uptake was reduced in the relatively large ischemic core and hypermetabolism was detected in the peri-infarct rim (Yuan et al. 2013). In the second study by Walberer et al., Wistar rats were subjected to a macrosphere model of irreversible ischemia (Gerriets et al. 2003), resulting in a reduced [^{18}F]FDG uptake only (Walberer et al. 2012). In contrast, by co-registration of PET with images from follow-up MRI, we found elevated [^{18}F]FDG uptake in the ischemic core (succumbing to infarction) and also in frontoparietal peri-infarct regions Fig 5A and 5B. These findings further corroborated our hypothesis that the model presented in Paper I preserve collateral flow in a way that more closely resembles human stroke. This was further demonstrated by the absence of hypermetabolism and CBF reduction in the ACA and PCA territories, whereas Yuan et al. report elevated uptake of [^{18}F]FDG in cortical regions supplied by the ACA and the PCA. This is expected since the model they used causes occlusion of the ACA and reduced flow in the PCA.

Furthermore we used co-registered PET and MRI data sets to generate time-activity curves from dynamic imaging data obtained from the region showing elevated [^{18}F]FDG. We found that the radioactivity within this region had a slower rate of increase, although reaching higher tissue radioactivity concentrations compared to the contralateral hemisphere, at the end of 90 minutes of M2CAO. Our interpretation of this is that the inflow of [^{18}F]FDG via the MCA is restricted by the reduction of CBF, but is compensated by collateral inflow of [^{18}F]FDG via the ACA and the PCA resulting in a elevated [^{18}F]FDG uptake at later time-points.

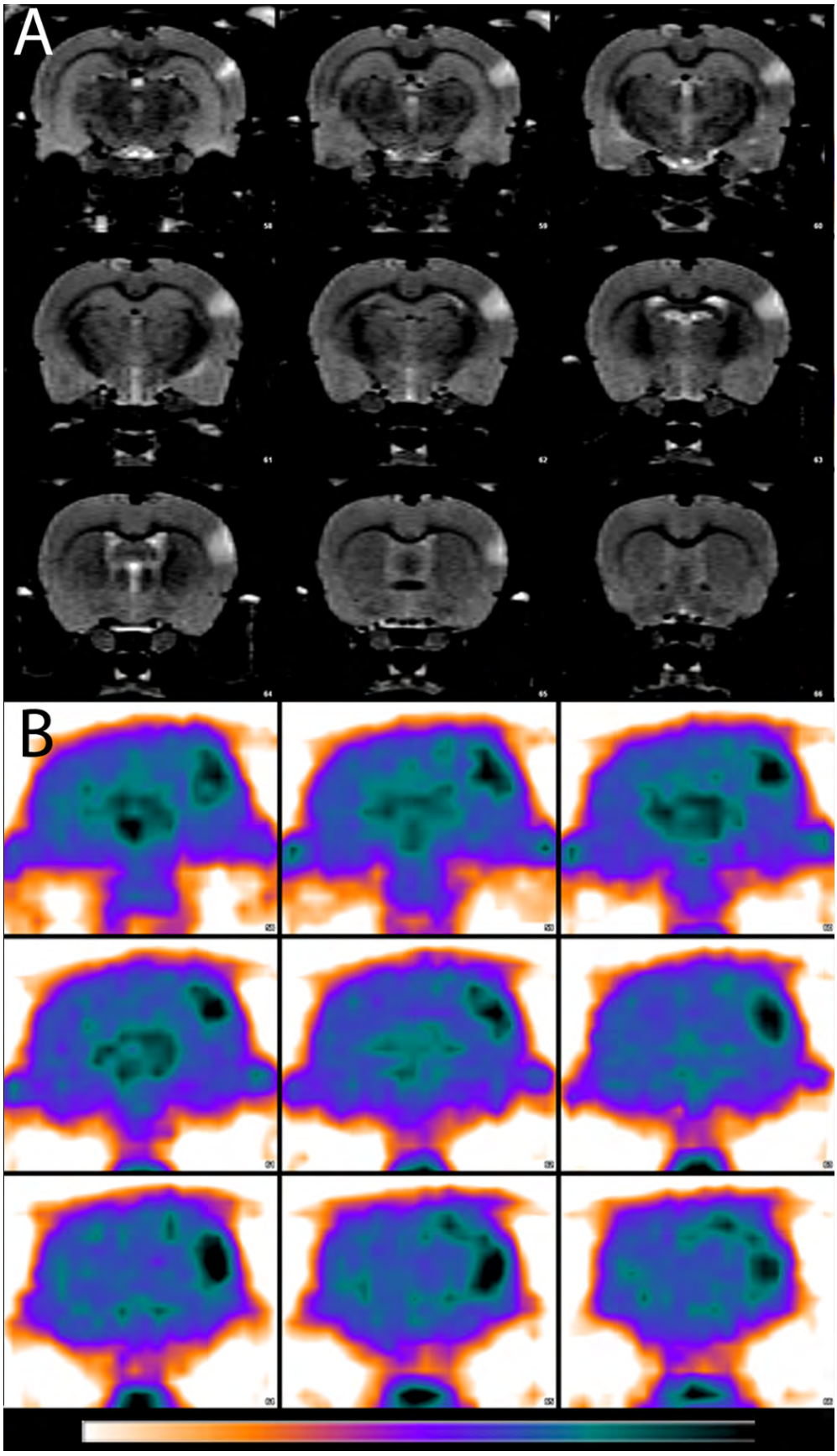

Fig. 5. T2WI- [^{18}F]FDG-PET images of ischemic stroke. (**A**) Coronal sections of the rat brain obtained by T2WI at 24 hours after 90 minutes of occlusion of the M2 segment of the middle cerebral artery (M2CAO), showing a focal cortical infarct. (**B**) [^{18}F]FDG-PET images, coronal sections co-registered with (**A**), summed over 90 minutes of M2CAO, showing increased uptake of [^{18}F]FDG distributed in the infarct and in peri-infarct regions.

In an effort to discriminate phosphorylation of [^{18}F]FDG from [^{18}F]FDG accumulation in the EC we applied Patlak compartmental analysis (Patlak et al. 1983). The compartmental analysis suggested that the presence of a significantly increased net flux of [^{18}F]FDG to the intracellular compartment during occlusion, indicating accelerated glycolysis as the mechanism behind elevated [^{18}F]FDG uptake. With MR spectroscopy we were able to detect increased levels of lactate in the ischemic core although not in peri-infarct regions. These results support previous findings indicating that [^{18}F]FDG hypermetabolism occurs under both aerobic and anaerobic conditions (Kita et al. 1995; Wise et al. 1983; Yuan et al. 2013).

Interestingly, current MRI research suggest that cessation of energy-dependent motion of intracellular contents is the predominant mechanism causing restricted diffusivity of water in acute cerebral ischemia (Duong et al. 1998), whereas our [^{18}F]FDG PET findings in hyperacute ischemic tissue showing restricted diffusion of tissue suggest an increase in metabolic activity. Speculatively, accelerated anaerobic glycolysis could occur in the ischemic brain regions displaying restricted diffusivity of water and that this acceleration would maintain energy-dependent mechanisms.

The cellular mechanisms of glucose metabolism in the brain remain highly controversial. As early as 1963 the Swedish scientist Hydén introduced the idea of a metabolic cooperation between neurons and glial cells (Hydén 1963). Since then it has become clear that astrocytes exhibit complex features in terms of glucose uptake and metabolism. Using technically advanced methods, Barros et al. were able to show that most glucose uptake in the cerebellum takes place in glial cells and not in Purkinje cells (Barros et al. 2009). In a recent study, glucose uptake was faster in hippocampal astrocytes than in neurons and the authors conclude that preferential glucose transport and metabolism occurs in glia (Jakoby et al. 2013). Furthermore, glucose metabolism in astrocytes is enhanced by glutamate (Voutsinos-Porche et al. 2003). Neuronal utilization of glucose increases only under excitotoxic conditions (Bak et al. 2009). Thus, evidence is mounting towards astrocytes being the main consumer of glucose and the main site for glycolysis as outlined in a review article by Pellerin (Bouzier-Sore & Pellerin 2013). The technical approach used in the present study may be very well suited for elucidating cellular contributions of altered glucose metabolism in ischemic stroke and to investigate therapeutic approaches aimed at the metabolic properties of astrocytes.

As the model was designed to include the possibility of reperfusion with the animal in the MR/PET-scanner, we also analysed spatiotemporal distribution of [^{18}F]FDG immediately after retraction of the occluding microwire. We then found that [^{18}F]FDG uptake was higher to the extent that an apparent lesion could be detected visually in all animals after 60 minutes of reperfusion. However, ROI analysis did not result in significant differences between the apparent lesion and the corresponding contralateral cortex. This finding was interpreted as cessation of glycolysis due to infarction.

Using ASL MRI, we found significant blood flow differences between the infarct and the adjacent brain regions. We interpreted these findings as a presence of an ischemic region and

a zone with reduced CBF supported by collateral flow. Since the occlusion model preserves collateral flow to a larger extent, compared to other models of stroke, the increased [^{18}F]FDG uptakes in tissue that later undergo infarction could thus represent a penumbral zone. To determine this, further experiments with reperfusion at earlier time-points are needed.

In order to validate whether the apparent lesions detected by MRI and PET actually represent tissue injury, we used immunohistochemistry to investigate the ischemic injury on the microscopic level. We found that apoptosis, defined by DNA fragmentation detected by TUNEL stainings, corresponded directly to the area of restricted diffusion displayed on DWI and also corresponded directly to the lesion defined by T2WI (Fig. 6). No TUNEL positive cells were detected outside of the regions showing a T2 signal increase. Within the lesion apparent on DWI and T2WI, the vast majority of cells showed DNA fragmentation. Thus, the apparent lesion defined by DWI and T2WI in our experimental setting is highly representative of cell death. Furthermore, we concluded that increased [^{18}F]FDG uptake occur both in dying cells as well as in cells not destined to die. Moreover, we conclude that lactate formation is evident in brain regions showing restricted diffusion and succumbing to infarction, whereas no or very little lactate is formed in regions adjacent to the regions displaying restricted diffusion albeit showing a reduction in CBF and increased [^{18}F]FDG uptake.

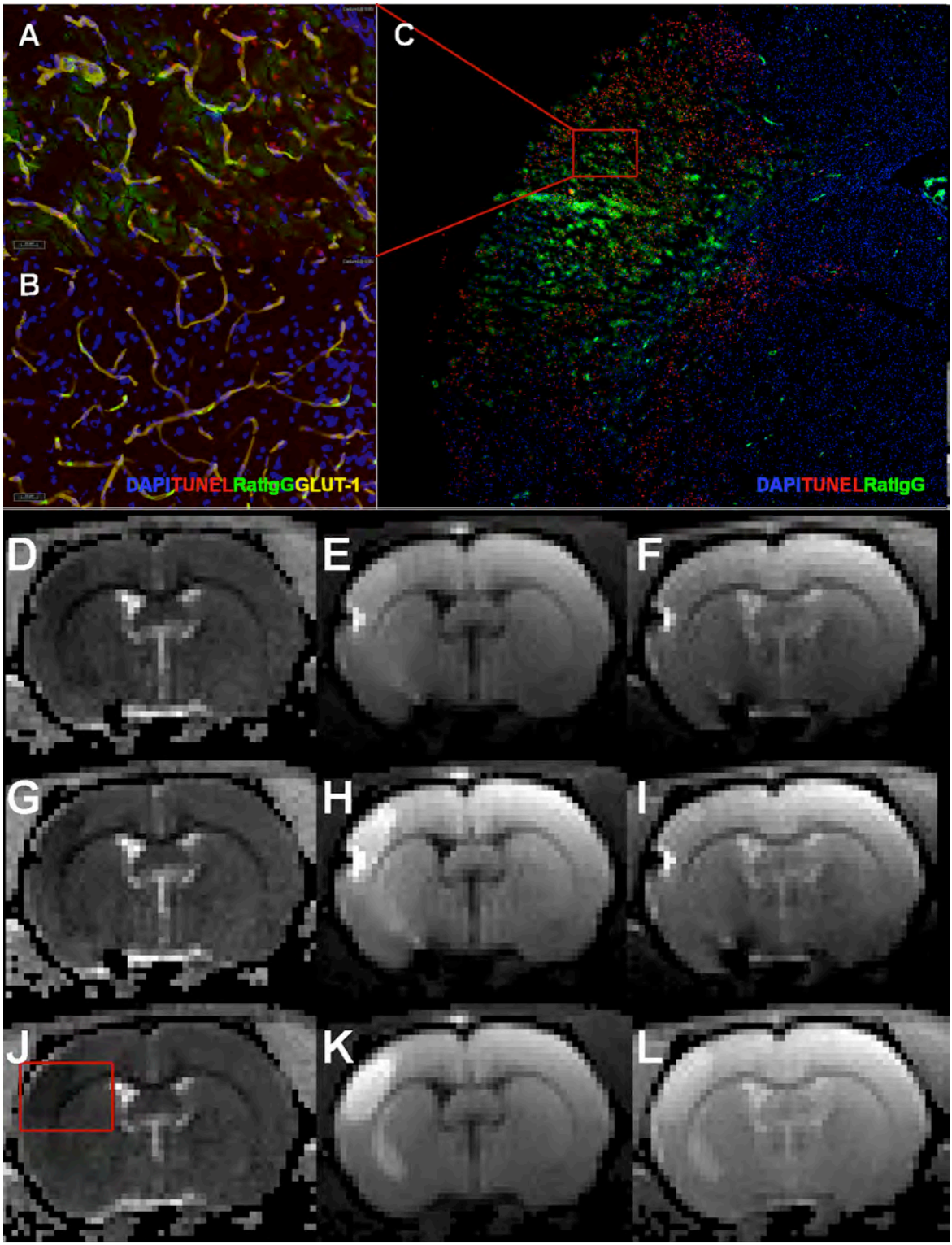

Fig. 6. Immunohistochemistry micrographs and diffusion-weighted imaging (DWI) of occlusion of the M2 segment of the middle cerebral artery (M2CAO) obtained from the same animal. (**A**) Micrograph (200X) of the ischemic core at 24 hours after 90 min M2CAO, showing apoptotic/necrotic cells (TUNEL, red), evidence of blood-brain barrier injury (Rat IgG, green), glucose transporters (GLUT-1, yellow) and cell nuclei (DAPI, blue). (**B**) Control image from normal contralateral cortex. (**C**) Micrograph (50X) of a coronal section corresponding to the red square in (**J**), showing apoptosis/necrosis (TUNEL, red), blood-brain barrier injury (ratIgG, green) and cell nuclei (DAPI, blue). (**D-L**) Left column = ADC map; middle column = b1000; right column =T2WI. (**D-F**) Images showing hyperacute infarction 15 minutes after M2CAO. The ischemic lesion is detected by DWI in **D** and **E.** The position of the nitinol microwire is revealed by a susceptibility artefact near the cortical surface. (**G-I**) Images from 90 minutes after M2CAO, showing an increase in diffusion restriction of water detected by a

decrease of the ADC and increased signal in the b1000 image reflecting cytotoxic edema. A slight increase in signal is detected by T2WI indicating an increased water content in the ischemic lesion. (**J**-**L**) Images obtained after 60 minutes of reperfusion, showing a markedly increased signal in T2WI reflecting vasogenic edema.

In summary, the model developed in Paper I resulted in spatiotemporal [^{18}F]FDG uptake characteristics different from what has been reported in studies using the intraluminal suture model. These differences were interpreted to be secondary to preservation of collateral flow and increase the possibilities to experimentally investigate metabolic events during ischemia and after reperfusion.

From a clinical perspective, it is well known that hyperglycemia (blood glucose concentration greater than 6.0 mmol/L) is prevalent in two-thirds of patients suffering from acute ischaemic stroke (Scott et al. 1999). It is also well known that hyperglycemia is concomitant with more severe ischemic strokes (Parsons et al. 2002). Whether hyperglycemia is a physiological response to acute ischemic stroke, or the result of poor glycaemic control secondary to diabetes preceding ischemic stroke and augmenting brain injury is, however, uncertain. As hyperglycemia has been observed concomitant with severe stroke, it was naturally considered as a therapeutic target (Stead et al. 2009). However, in a recent clinical trial (INSULINFARCT) in which insulin treatment was used in patients presenting with acute ischemic stroke, a poorer outcome in the normoglycemic control group was, somewhat surprisingly, observed (Rosso et al. 2012). A recent review by Cochrane concluded that there is no current evidence for controlling hyperglycemia in acute ischemic stroke and the authors of the INSULINFARCT trial encouraged a reappraisal of the pathophysiological models of glucose energy metabolism alterations in focal cerebral ischemia (Rosso et al. 2012; Bellolio et al. 2014). Our results confirm the findings reported in the experimental body of work on infarct-related glucose hypermetabolism and extend them to also include hypermetabolism of glucose occurring in the ischemic core at hyperacute stages when preserved collateral flow is present. These findings indicate the presence of a protective pathophysiological mechanism, in which the brain extracts greater amounts of glucose when subjected to ischemia in order to meet increased energy demands. Such a mechanism could plausibly be facilitated by higher levels of blood glucose and could potentially be negatively influenced by insulin treatment, explaining the results from the INSULINFARCT trial. It could also be hypothesized that poor glycemic control previous to an ischemic insult could derail this protective pathophysiological response, worsening ischemic brain injury.

4.4 ANTI VEGF-B TREATMENT OF ISCHEMIC STROKE (PAPER IV)

In Paper IV, we used the model developed in Paper I and the imaging protocols established in Paper III to investigate potential neuroprotective effects of pre-treatment with an anti-VEGF-B antibody. The rationale of pre-treating with anti-VEGF-B antibody is explained by recent evidence showing that VEGF-B antagonism alters the metabolic barrier function of the endothelium (Hagberg et al. 2012; Hagberg et al. 2013; Hagberg et al. 2010). For such alterations to come into full effect, administration of anti-VEGF-B antibody may need to be performed before an ischemic stroke. This situation would be the case as VEGF-B antagonism has been proposed as a promising strategy to treat type-2 diabetes (Hagberg et al. 2012), a patient group with increased risk of ischemic stroke. Furthermore, as it was found that pre-treatment with anti-VEGF-B antibody ameliorated the ischemic injury in a photothrombotic mouse model, we wanted to investigate whether this result would be reproduced in the experimental setting developed in this thesis (Nilsson & Su 2015).

Compared to control rats, infarct volumes in rats receiving pre-treatment with anti-VEGF-B antibody were significantly smaller at 24 hours and at 7 days after ischemic stroke. Furthermore, in anti-VEGF-B antibody treated rats, the decrease in infarct volume between the 24-hour end-point and 7 days was statistically significant, whereas no significant reduction of infarct volume could be detected in the control group. Our findings thus confirmed previous results in mice, in which smaller infarct volumes were observed following one week pre-treatment with anti-VEGF-B antibody (Nilsson & Su 2015).

The decrease in apparent lesion volume between 24 hours and 7 days in the anti-VEGF-B antibody treated group, as defined by T2WI, could be explained by an enhanced recovery of the ischemic border zone, where VEGF-B previously has been shown to upregulate (Xie et al. 2013). Neutralizing VEGF-B in this region could hypothetically facilitate mechanisms responsible for re-distribution of cerebral edema. Another explanation for this finding could be that VEGF-B antagonism enhances the functionality of endothelium under ischemic stress causing quicker recovery of the disrupted blood-brain barrier. In any case, an enhanced reduction of cerebral edema at an early stage after recanalization therapy would be of significant clinical importance. Cerebral edema is frequently encountered in patients suffering from severe ischemic stroke. Recently, cerebral edema has also been recognized as an independent predictor of poor outcome in moderately-sized ischemic stroke (Battey et al. 2014). Following acute ischemic stroke, cerebral edema develops early in the course of clinical deterioriation, which makes the condition an appealing target for therapeutic intervention.

As VEGF-B has been proposed as an important player in the endothelial transport of lipids and carbohydrates (Hagberg et al. 2010), we investigated whether treatment with anti-VEGF-B antibodies would change [^{18}F]FDG uptake characteristics. Furthermore, we assessed regional CBF to assess whether VEGF-B antagonism would have any effects on perfusion. However, with the experimental setup used in our study, we were unable to detect any differences between the groups regarding [^{18}F]FDG uptake or perfusion. There was a

tendency towards a more pronounced increase in CBF between 24 hours and 7 days in the anti-VEGF-B treated group although not reaching statistical significance.

In summary, the findings in Paper IV suggest that neutralization of VEGF-B results in smaller infarcts, extending and confirming previous results in a mice (Nilsson & Su 2015). Considering, in-vivo imaging of glucose metabolism and cerebral blood flow did not provide any indications of a mechanistic explanation of the observed reduction in infarct volume, further investigations on a microscopic level are needed to reveal potential tissue alterations resulting in resistance to ischemia. Furthermore, we found a significant regression of infarct volume in the anti-VEGF-B treated group between the two time points. This regression may reflect an enhanced recovery of the ischemic border zone, where VEGF-B has been shown to upregulate and that this region would be viable enough to regulate vasogenic edema. Another explanation for this finding could be that VEGF-B antagonism enhances the functionality of the endothelium resulting in a quicker recovery of a leaky blood-brain barrier.

5 GENERAL CONCLUSIONS

1. Translation of clinical endovascular techniques to the bench provides possibilities to refine experimental procedures for accessing and perturbing the cerebrovascular system in the rat.

2. Under experimental conditions, hypermetabolism of glucose occurs both in the ischemic core and in peri-infarct regions and under aerobic and anaerobic conditions.

3. In acute cerebral ischemia, hypermetabolism of glucose occurs in parallel with- and in the same brain tissue that display restricted diffusion. As the current paradigm of the diffusion restriction attributes cessation of energy-dependent motion of intracellular contents as the main mechanism, we suggest that the energy generated from accelerated glycolysis is dedicated to support cellular respiration.

4. Treatment with antibodies against VEGF-B in result in reduction of infarct volume. and also causes a faster normalization of the T2WI lesion during the first post-ischemic week.

6 ACKNOWLEDGMENTS

I would like to express my sincerest gratitude to:

Staffan Holmin, my supervisor. With his professionalism, his inspiration and his remarkable ability to understand very quickly a problem and make relevant recommendations, he has expertly guided me through this thesis work.

Michael Söderman, co-supervisor, for support and encouragement, and for his contribution in developing the experimental angiography and intervention laboratory.

Sharon Stone-Elander, for introducing me to the wonders of PET and radiochemistry.

Johan Lundberg, for friendship, for *epic* experiments and for endless conversations spanning everything from building insulation to rocket propulsion.

My brilliant co-authors, it has been a true privilege and a great pleasure working with all of you: **Peter Damberg** and **Sahar Nikkhou-Aski**, for patience and for adventures in high-field MRI. **Erik Samén**, **Li Lu** and **Jonas Grafström**, for exciting PET experiments. **Philip Little**, for paying the iron price, linguistic assistance and for interesting discussions. **Nicholas Mitsios** and **Jan Mulder**, for professionalism and high-tech visualization of immunohistochemistry. **Ulf Eriksson**, **Linda Fredriksson** and **Ingrid Nilsson**, for providing insights into endothelial functions and on how cutting-edge research is performed.

Stefan Jonsson, **Nasreen Jaff**, and **Rikard Grankvist** for friendship, excellent scientific skills and interesting discussions.

Johanna Doshé and **Ulrika Nilsson** for showing me how neurointerventional procedures are performed properly.

The radiochemistry group, especially **Jan-Olov Thorell** and **Emma Jussing** for teaching me about radiochemistry and providing radiotracers.

Ann-Christin Eklöf, **Ann-Christin Sandberg-Nordqvist** and **Pellina Jansson** for creating and maintaining a fantastic research environment at KERIC.

The staff at AKM, especially **Mirre** for keeping track of all the paperwork, **Leo** for repairing and modifying the ZEISS and **Linda** for helping out when my Th4 was fractured.

All former and present colleagues at KERIC: **Anton**, **Yahor**, **Jiangning**, **Jack**, **Attila**, **Cyril**, **Adam**, **Kálmán**, **Jenny**, **Sara** and **Zsolt**, for friendship and help.

Caroline Gahm, **Tiit Mathiesen** and **Britt Meijer** at the neurosurgical lab, for introducing me to neuroscience, immunohistochemistry, the writing of scientific papers and on how to respond to peer reviewers' comments.

Jonathan Nordblom, for friendship, for expanding my views on politics and culture and for great pieces of life advice.

Ragnhild Hjertberg, for keeping my daughters safe and for calming my mind.

All colleagues and coworkers at the Departments of Radiology and Neuroradiology, for showing an interest in my work. I especially thank **Lennart Blomqvist** for mentorship. Also thank you to **Peter Lindholm**, **Fredrik Strand** and **Anders Sundin** for expert advice and interesting discussions.

Marianne, **Tomi** and **Toril**, for caring. **Jenny**, **Moritz**, **Alma** and **Heidi**, for all the fun.

Filip, **Alexandra**, **Edit** and **Liv**; **Kasper**, **Camilla**, **Sondre**, **Astrid** and **Hjalmar**, for love and support. **My** and **Jonatan**, my siblings, I love you.

My mother **Anita** and my father **Olof**, for believing in me and for raising me to be confident and self-reliant.

Jessika, my Love, all I need is the light of your smile. This thesis is dedicated to you and to our children ***Elmer***, ***Tyra*** and ***Hedvig***, with love and gratitude.

7 REFERENCES

Astrup, J. et al., 1977. Cortical evoked potential and extracellular K+ and H+ at critical levels of brain ischemia. *Stroke*, 8(1), pp.51–57.

Bak, L.K. et al., 2009. Neuronal glucose but not lactate utilization is positively correlated with NMDA-induced neurotransmission and fluctuations in cytosolic Ca 2+levels. *Journal of Neurochemistry*, 109, pp.87–93.

Barros, L.F. et al., 2009. Preferential transport and metabolism of glucose in Bergmann glia over Purkinje cells: A multiphoton study of cerebellar slices. *Glia*, 57(9), pp.962–970.

Battey, T.W.K. et al., 2014. Brain edema predicts outcome after nonlacunar ischemic stroke. *Stroke*, 45(12), pp.3643–3648.

Bederson, J.B. et al., 1986. Rat middle cerebral artery occlusion: evaluation of the model and development of a neurologic examination. *Stroke*, 17(3), pp.472–476.

Belayev, L. et al., 1996. Middle cerebral artery occlusion in the rat by intraluminal suture. Neurological and pathological evaluation of an improved model. *Stroke*, 27(9), pp.1616–22.

Belayev, L. et al., 1997. Transient middle cerebral artery occlusion by intraluminal suture: I. Three-dimensional autoradiographic image-analysis of local cerebral glucose metabolism-blood flow interrelationships during ischemia and early recirculation. *Journal of Cerebral Blood flow and Metabolism,* 17(12), pp.1266–1280.

Bellolio, M.F., Gilmore, R.M. & Ganti, L., 2014. Insulin for glycaemic control in acute ischaemic stroke. *Cochrane database of systematic reviews (Online)*, 1, p.CD005346.

Berkhemer, O.A. et al., 2015. A Randomized Trial of Intraarterial Treatment for Acute Ischemic Stroke. *New England Journal of Medicine*, 372(1), pp.11–20.

Blennow, M. et al., 1995. Early [18F] FDG positron emission tomography in infants with hypoxic-ischaemic encephalopathy shows hypermetabolism during the postasphyctic period. *Acta Paediatrica*, 84(11), pp.1289–1295.

Bloch, F., 1946. Nuclear induction. *Physical review*.

Bouzier-Sore, A.-K. & Pellerin, L., 2013. Unraveling the complex metabolic nature of astrocytes. *Frontiers in Cellular Neuroscience*, 7, p.179.

Brott, T. et al., 1989. Measurements of acute cerebral infarction: lesion size by computed tomography. *Stroke*, 20(7), pp.871–875.

Brown, J.O., 1966. The morphology of circulus arteriosus cerebri in rats. *The Anatomical Record*, 156(1), pp.99–106.

Bruno, A., Williams, L.S. & Kent, T.A., 2004. How important is hyperglycemia during acute brain infarction? *The Neurologist*, 10(4), pp.195–200.

Buhalog, A. et al., 2010. A Method for Serial Selective Arterial Catheterization and Digital Subtraction Angiography in Rodents. *Blood*, 31(8), pp.1508–1511.

Calamante, F. et al., 1999. Early changes in water diffusion, perfusion, T1, and T2 during focal cerebral ischemia in the rat studied at 8.5 T. *Magnetic Resonance in Medicine*, 41(3), pp.479–485.

Campbell, B.C.V. et al., 2013. A multicenter, randomized, controlled study to investigate EXtending the time for Thrombolysis in Emergency Neurological Deficits with Intra-Arterial therapy (EXTEND-IA). *International Journal of Stroke*, 9(1), pp.126–132.

Carmichael, S.T., 2006. Cellular and molecular mechanisms of neural repair after stroke: Making waves. *Annals of Neurology*, 59(5), pp.735–742.

Carmichael, S.T., 2005. Rodent models of focal stroke: size, mechanism, and purpose. *NeuroRx*, 2(3), pp.396–409.

Carmichael, S.T. et al., 2004. Evolution of diaschisis in a focal stroke model. *Stroke*, 35(3), pp.758–763.

Chen, L., Magliano, D.J. & Zimmet, P.Z., 2012. The worldwide epidemiology of type 2 diabetes mellitus--present and future perspectives. *Nature reviews. Endocrinology*, 8(4), pp.228–236.

Choki, J. et al., 1984. Correlation between brain surface potassium and glucose utilization after bilateral cerebral ischemia in the gerbil. *Stroke*, 15(5), pp.851–857.

Dirnagl, U. & Fisher, M., 2012. International, multicenter randomized preclinical trials in translational stroke research: It's time to act. *Journal of Cerebral Blood Flow & Metabolism*, 32(6), pp.933–935.

Dittmar, M. et al., 2003. External Carotid Artery Territory Ischemia Impairs Outcome in the Endovascular Filament Model of Middle Cerebral Artery Occlusion in Rats. *Stroke*, 34(9), pp.2252–2257.

Divani, A.A. et al., 2015. Focal middle cerebral artery ischemia in rats via a transfemoral approach using a custom designed microwire. *Journal of NeuroInterventional Surgery*.

Duong, T.Q. et al., 1998. Evaluation of extra- and intracellular apparent diffusion in normal and globally ischemic rat brain via 19F NMR. *Magnetic Resonance in Medicine*, 40(1), pp.1–13.

Durukan, A. & Tatlisumak, T., 2007. Acute ischemic stroke: overview of major experimental rodent models, pathophysiology, and therapy of focal cerebral ischemia. *Pharmacology, Biochemistry, and Behavior*, 87(1), pp.179–197.

Endres, M. et al., 2008. Improving Outcome after Stroke: Overcoming the Translational Roadblock. *Cerebrovascular Disease*, 25(3), pp.268–278.

Feigin, V.L. et al., 2014. Global and regional burden of stroke during 1990-2010: findings from the Global Burden of Disease Study 2010. *Lancet*, 383(9913), pp.245–254.

Ferrara, N. & Henzel, W.J., 1989. Pituitary follicular cells secrete a novel heparin-binding growth factor specific for vascular endothelial cells. *Biochemical and Biophysical Research Communications*, 161(2), pp.851–858.

Gaál, E.I. et al., 2013. Comparison of vascular growth factors in the murine brain reveals

placenta growth factor as prime candidate for CNS revascularization. *Blood*, 122(5), pp.658–665.

Gerriets, T. et al., 2003. The macrosphere model: evaluation of a new stroke model for permanent middle cerebral artery occlusion in rats. *Journal of Neuroscience Methods*, 122(2), pp.201–211.

Ginsberg, M.D. & Busto, R., 1989. Rodent models of cerebral ischemia. *Stroke*, 20(12), pp.1627–1642.

Ginsberg, M.D. et al., 1977. Local glucose utilization in acute focal cerebral ischemia: Local dysmetabolism and diaschisis. *Neurology*, 27(11), pp.1042–1042.

Ginsberg, M.D., Graham, D.I. & Busto, R., 1985. Regional glucose utilization and blood flow following graded forebrain ischemia in the rat: correlation with neuropathology. *Annals of Neurology*, 18(4), pp.470–481.

Goyal, M. et al., 2015. Randomized Assessment of Rapid Endovascular Treatment of Ischemic Stroke. *New England Journal of Medicine*, 372(11), pp.1019–1030.

Greenberg, D.A. & Jin, K., 2013. Vascular endothelial growth factors (VEGFs) and stroke. *Cellular and molecular life sciences*, 70(10), pp.1753–1761.

Guan, W. et al., 2011. Vascular protection by angiotensin receptor antagonism involves differential VEGF expression in both hemispheres after experimental stroke. *PLoS ONE*, 6(9), p.e24551.

Hagberg, C. et al., 2013. Endothelial Fatty Acid Transport: Role of Vascular Endothelial Growth Factor B. *Physiology*, 28(2), pp.125–134.

Hagberg, C.E. et al., 2012. Targeting VEGF-B as a novel treatment for insulin resistance and type 2 diabetes. *Nature*, 490(7420), pp.426–430.

Hagberg, C.E. et al., 2010. Vascular endothelial growth factor B controls endothelial fatty acid uptake. *Nature*, 464(7290), pp.917–921.

Hamberger H & Hydén H, 1963. Inverse enzymatic changes in neurons and glia during increased function and hypoxia. *The Journal of Cell Biology*, 16, pp.521–525.

Hayashi, T. et al., 1997. Rapid Induction of Vascular Endothelial Growth Factor Gene Expression After Transient Middle Cerebral Artery Occlusion in Rats. *Stroke*, 28(10), pp.2039–2044.

Heiss, W.-D., 2011. The Ischemic Penumbra: Correlates in Imaging and Implications for Treatment of Ischemic Stroke. *Cerebrovascular Disease*, 32(4), pp.307–320.

Jakoby, P. et al., 2013. Higher Transport and Metabolism of Glucose in Astrocytes Compared with Neurons: A Multiphoton Study of Hippocampal and Cerebellar Tissue Slices. *Cerebral Cortex*, 24(1), pp.222–231.

Kanemitsu, H. et al., 2002. Differences in the Extent of Primary Ischemic Damage Between Middle Cerebral Artery Coagulation and Intraluminal Occlusion Models. *Journal of Cerebral Blood Flow & Metabolism*, 22(10), pp.1196–1204.

Kimura, R. et al., 2005. Vascular Endothelial Growth Factor Antagonist Reduces Brain Edema Formation and Venous Infarction. *Stroke*, 36(6), pp.1259–1263.

Kissela, B.M. et al., 2012. Age at stroke: temporal trends in stroke incidence in a large, biracial population. *Neurology*, 79(17), pp.1781–1787.

Kissela, B.M. et al., 2005. Epidemiology of ischemic stroke in patients with diabetes: the greater Cincinnati/Northern Kentucky Stroke Study. *Diabetes Care*, 28(2), pp.355–359.

Kita, H. et al., 1995. Cerebral blood flow and glucose metabolism of the ischemic rim in spontaneously hypertensive stroke-prone rats with occlusion of the middle cerebral artery. *Journal of Cerebral Blood flow and Metabolism*, 15(2), pp.235–241.

Koizumi, G. et al., 1986. Experimental Studies of Ischemic Brain Edema: I: a New Experimental Model of Cerebral Embolism in Rats in Which Recirculation Can Be Introduced in the Ischemic Area. *Japan Journal of Stroke*, 8(1), p.8.

Komatsumoto, S. et al., 1989. Local cerebral glucose utilization in chronic middle cerebral artery occlusion in the cat. *Journal of Cerebral Blood flow and Metabolism*, 9(4), pp.535–547.

Kovacs, Z. et al., 1996. VEGF and flt: Expression Time Kinetics in Rat Brain Infarct. *Stroke*, 27(10), pp.1865–1873.

Lennmyr, F. et al., 1998. Expression of vascular endothelial growth factor (VEGF) and its receptors (Flt-1 and Flk-1) following permanent and transient occlusion of the middle cerebral artery in the rat. *Journal of Neuropathology and Experimental Neurology*, 57(9), pp.874–882.

Li, Y. et al., 2008. VEGF-B inhibits apoptosis via VEGFR-1-mediated suppression of the expression of BH3-only protein genes in mice and rats. *Journal of Clinical Investigation*, 118(3), pp.913–923.

Liu, F., Schafer, D.P. & McCullough, L.D., 2009. TTC, fluoro-Jade B and NeuN staining confirm evolving phases of infarction induced by middle cerebral artery occlusion. *Journal of Neuroscience Methods*, 179(1), pp.1–8.

Longa, E.Z. et al., 1989. Reversible middle cerebral artery occlusion without craniectomy in rats. *Stroke*, 20(1), pp.84–91.

Lythgoe, M.F. et al., 2000. Acute changes in MRI diffusion, perfusion, T(1), and T(2) in a rat model of oligemia produced by partial occlusion of the middle cerebral artery. *Magnetic Resonance in Medicine*, 44(5), pp.706–712.

Macrae, I.M., 1992. New models of focal cerebral ischaemia. *British Journal of Clinical Pharmacology*, 34(4), p.302.

Markus, R. et al., 2004. Hypoxic tissue in ischaemic stroke: persistence and clinical consequences of spontaneous survival. *Brain*, 127(6), pp.1427–1436.

Medin, J. et al., 2004. Increasing stroke incidence in Sweden between 1989 and 2000 among persons aged 30 to 65 years: evidence from the Swedish Hospital Discharge Register. *Stroke*, 35(5), pp.1047–1051.

Mergenthaler, P. & Meisel, A., 2012. Do stroke models model stroke? *Disease models & mechanisms*, 5(6), pp.718–725.

Molina, C.A. et al., 2013. REVASCAT: a randomized trial of revascularization with SOLITAIRE FR® device vs. best medical therapy in the treatment of acute stroke due to anterior circulation large vessel occlusion presenting within eight-hours of symptom onset. *International Journal of Stroke*, 10(4), pp.619–626.

Moseley, M.E. et al., 1990. Early detection of regional cerebral ischemia in cats: comparison of diffusion- and T2-weighted MRI and spectroscopy. *Magnetic Resonance in Medicine*, 14(2), pp.330–346.

Nakai, H. et al., 1987. Simultaneous in vivo measurement of lumped constant and rate constants in experimental cerebral ischemia using F-18 FDG. *Stroke*, 18(1), pp.158–167.

Nakai, H. et al., 1988. Triple-tracer autoradiography demonstrates effects of hyperglycemia on cerebral blood flow, pH, and glucose utilization in cerebral ischemia of rats. *Stroke*, 19(6), pp.764–772.

Nasu, S. et al., 2002. Evaluation of 18F-FDG PET in acute ischemic stroke: assessment of hyper accumulation around the lesion. *Kaku igaku. The Japanese journal of nuclear medicine*, 39(2), pp.103–110.

Nedergaard, M., Gjedde, A. & Diemer, N.H., 1986. Focal ischemia of the rat brain: autoradiographic determination of cerebral glucose utilization, glucose content, and blood flow. *Journal of Cerebral Blood flow and Metabolism*, 6(4), pp.414–424.

Nilsson, I. & Su, E.J., 2015. Targeting VEGF-B in Ischemic Stroke *(Manuscript)*.

Norris, D.G., Niendorf, T. & Leibfritz, D., 1994. Healthy and infarcted brain tissues studied at short diffusion times: The origins of apparent restriction and the reduction in apparent diffusion coefficient. *NMR in Biomedicine*, 7(7), pp.304–310.

Parsons, M.W. et al., 2002. Acute hyperglycemia adversely affects stroke outcome: a magnetic resonance imaging and spectroscopy study. *Ann Neurol*, 52(1), pp.20–28.

Patlak, C.S., Blasberg, R.G. & Fenstermacher, J.D., 1983. Graphical evaluation of blood-to-brain transfer constants from multiple-time uptake data. *Journal of Cerebral Blood flow and Metabolism*, 3(1), pp.1–7.

Phelps, M.E., 1981. Positron computed tomography studies of cerebral glucose metabolism in man: theory and application in nuclear medicine. *Seminars in nuclear medicine*, 11(1), pp.32–49.

Rosso, C. et al., 2012. Intensive Versus Subcutaneous Insulin in Patients With Hyperacute Stroke: Results From the Randomized INSULINFARCT Trial. *Stroke*, 43(9), pp.2343–2349.

Sako, K. et al., 1985. Correlation of local cerebral blood flow, glucose utilization, and tissue pH following a middle cerebral artery occlusion in the rat. *Stroke*, 16(5), pp.828–834.

Sappey-Marinier, D. et al., 1992. Proton magnetic resonance spectroscopy of human brain:

Applications to normal white matter, chronic infarction, and MRI white matter signal hyperintensities. *Magnetic Resonance in Medicine*, 26(2), pp.313–327.

Saver, J.L. et al., 2015. Solitaire™ with the Intention for Thrombectomy as Primary Endovascular Treatment for Acute Ischemic Stroke (SWIFT PRIME) trial: protocol for a randomized, controlled, multicenter study comparing the Solitaire revascularization device with IV tPA with IV t. *International Journal of Stroke*, 10(3), pp.439–448.

Schneider, C.A., Rasband, W.S. & Eliceiri, K.W., 2012. NIH Image to ImageJ: 25 years of image analysis. *Nature Methods*, 9(7), pp.671–675.

Schuier, F.J. & Hossmann, K.A., 1980. Experimental brain infarcts in cats. II. Ischemic brain edema. *Stroke*, 11(6), pp.593–601.

Scott, J.F. et al., 1999. Prevalence of admission hyperglycaemia across clinical subtypes of acute stroke. *The Lancet*, 353(9150), pp.376–377.

Scremin, O.U., 1995. *Cerebral Vascular System*, The rat nervous system.

Senger, D. et al., 1983. Tumor cells secrete a vascular permeability factor that promotes accumulation of ascites fluid. *Science*, 219(4587), pp.983–985.

Shimamura, N. et al., 2006. Comparison of silicon-coated nylon suture to plain nylon suture in the rat middle cerebral artery occlusion model. *Journal of Neuroscience Methods*, 156(1-2), pp.161–165.

Shimamura, N. et al., 2009. Novel rat middle cerebral artery occlusion model: Trans-femoral artery approach combined with preservation of the external carotid artery. *Journal of Neuroscience Methods*, 184(2), pp.195–198.

Solomon, S.B., 2005. Incorporating CT, MR Imaging, and Positron Emission Tomography into Minimally Invasive Therapies. *Journal of Vascular and Interventional Radiology*, 16(4), pp.445–447.

Solomon, S.B. & Silverman, S.G., 2010. Imaging in Interventional Oncology. *Radiology*, 257(3), pp.624–640.

Stead, L.G. et al., 2009. Hyperglycemia as An Independent Predictor of Worse Outcome in Non-diabetic Patients Presenting with Acute Ischemic Stroke. *Neurocritical Care*, 10(2), pp.181–186.

Sun, F. et al., 2005. Transfemoral selective “intraluminal wiring” technique for transient middle cerebral artery occlusion in rats. *Journal of Neuroscience Methods*, 149(1), pp.82–89.

Sun, Y. et al., 2004. Increased severity of cerebral ischemic injury in vascular endothelial growth factor-B-deficient mice. *Journal of Cerebral Blood flow and Metabolism*, 24(10), pp.1146–1152.

Taheri, S. et al., 2014. Isoflurane reduces the ischemia reperfusion injury surge: a longitudinal study with MRI. *Brain Research*, 1586, pp.173–183.

Voutsinos-Porche, B. et al., 2003. Glial glutamate transporters mediate a functional metabolic crosstalk between neurons and astrocytes in the mouse developing cortex.

Neuron, 37(2), pp.275–286.

Walberer, M. et al., 2012. Potential of early [(18)F]-2-fluoro-2-deoxy-D-glucose positron emission tomography for identifying hypoperfusion and predicting fate of tissue in a rat embolic stroke model. *Stroke*, 43(1), pp.193–198.

Welsh, F.A. et al., 1980. Correlation between glucose utilization and metabolite levels during focal ischemia in cat brain. *Stroke*, 11(1), pp.79–84.

Wise, R.J.S. et al., 1983. Disturbance of oxidative metabolism of glucose in recent human cerebral infarcts. *Annals of Neurology*, 14(6), pp.627–637.

Xie, L. et al., 2013. Vascular endothelial growth factor-B expression in postischemic rat brain. *Vascular Cell*, 5(1), p.8.

Yuan, H. et al., 2013. Spatiotemporal uptake characteristics of [18]F-2-fluoro-2-deoxy-D-glucose in a rat middle cerebral artery occlusion model. *Stroke*, 44(8), pp.2292–2299.

Yushkevich, P.A. et al., 2006. User-guided 3D active contour segmentation of anatomical structures: significantly improved efficiency and reliability. *NeuroImage*, 31(3), pp.1116–1128.

Zaharchuk, G., 2014. Arterial spin-labeled perfusion imaging in acute ischemic stroke. *Stroke*, 45(4), pp.1202–1207.

Zhang, Z.G. et al., 2000. VEGF enhances angiogenesis and promotes blood-brain barrier leakage in the ischemic brain. *Journal of Clinical Investigation*, 106(7), pp.829–838.